Longitudinal calcium imaging of VIP interneuron circuits reveals shifting response fidelity dynamics in the stroke damaged brain

by

Mohammad Motaharinia
B.Sc., University of Isfahan, 2015

A Thesis Submitted in Partial Fulfillment
of the Requirements for the Degree of

MASTER OF SCIENCE

in the Division of Medical Sciences (Neuroscience)

Supervisory Committee

Longitudinal calcium imaging of VIP interneuron circuits reveals shifting response fidelity dynamics in the stroke damaged brain

by

Mohammad Motaharinia
B.Sc., University of Isfahan, 2015

Supervisory Committee

Dr. Craig E. Brown (Division of Medical Sciences)
Supervisor

Dr. Patrick Nahirney (Division of Medical Sciences)
Departmental Member

Dr. Kerry R. Delaney (Department of Biology)
Outside Member

Abstract

Although inhibitory cortical interneurons play a critical role in regulating brain excitability and function, the effects of stroke on these neurons is poorly understood. In particular, interneurons expressing vasoactive intestinal peptide (VIP) specialize in inhibiting other classes of inhibitory neurons, and thus serve to modulate cortical sensory processing. To understand how stroke affects this circuit, we imaged VIP neuron responses (using GCaMP6s) to low and high intensity forepaw stimulation, both before and after focal stroke in somatosensory cortex. Our data show that the fraction of forelimb responsive VIP interneurons and their response fidelity (defined as a cell's number of responsive trials out of eight trials at a certain imaging week) was significantly reduced in the first week after stroke, especially when lower intensity forepaw stimulation was employed. The loss of responsiveness was most evident in highly active VIP neurons (defined by their level of responsiveness before stroke), whereas less active neurons were minimally affected. Of note, a small fraction of VIP neurons that were minimally active before stroke, became responsive afterwards suggesting that stroke may unmask sensory responses in some neurons. Although VIP responses to forepaw stimulation generally improved from 2-5 weeks recovery, the variance in response fidelity after stroke was comparatively high and therefore less predictable than that observed before stroke. Lastly, stroke related changes in response properties were restricted to within 400μm of the infarct border. These findings reveal the dynamic and resilient nature of VIP neurons and suggest that a sub-population of these cells are more apt to lose sensory responsiveness during the initial phase of stroke, whereas some minimally responsive cells are progressively recruited into the forelimb sensory circuit.

Furthermore, stroke appears to disrupt the predictability of sensory-evoked responses in these cortical interneurons which could have important consequences for sensory perception.

Table of Contents

List of Tables

List of Figures

Acknowledgments

I would like to especially thank my supervisor Dr. Craig Brown, who provided me with the opportunity to work in the research field that I have always been most passionate about. I am deeply grateful for your support, guidance and everything I learned from you.

I would like to thank my supervisory committee Dr. Kerry Delaney and Dr. Patrick Nahirney for their guidance on my project and all the support they gave me throughout the duration of my project.

My beautiful family, who have always given me the best of love, courage and motivation. I love you from the bottom of my heart. My amazing lab mates, Emily White, Roobina Boghozian, Sorabh Sharma, Essie Mehina, Ben Schager, Alejandra Raudales, Sunny Choi, Farnoosh Farhoomand, Sima Abbasi, Reza Zamani, Manjinder Cheema. I was so lucky to work in the same place with you guys. Thanks for all the friendship and the pleasant time we had together. To my friend Patrick Reeson, working with you was a real honor for me, thanks for everything.

I also would like to thank all previous members of Brown lab, Stephanie Taylor, Kim Gerrow, Kelly Tennant, Kevin Yongblah, Leila Gholami, and all my friends in the Division of Medical Sciences and Biology Department.

Dedication

To my kindest dad and mom who

taught me the real meaning of dedication.

Abbreviations

AAV Adeno-associated virus

ACSF Artificial cerebrospinal fluid

ANOVA Analysis of variance

AVG Average

BL Baseline

CCD Charge-coupled device

cRT-PCR Competitive reverse transcription-polymerase chain reaction

DMCM Methyl-6,7-dimethoxy-4-ethyl-beta-carboline-3-carboxylate

DREADDs Designer receptor exclusively activated by designer drugs

FL Forelimb

FLM1 Primary forelimb motor cortex

FLS1 Primary forelimb somatosensory cortex

GABA Gamma-aminobutyric acid

GAD Glutamate decarboxylase

GCaMP6s A genetically encoded calcium indicator created from fusion of a Green fluorescent protein, Calmodulin protein, and M13 peptide

GECI Genetically encoded calcium indicator

HL Hindlimb

HLS1 Primary hindlimb somatosensory cortex

IOS Intrinsic optical signal

LSCI Laser speckle contrast imaging

LTP	Long-term potentiation
M1	Primary motor cortex
MCA	Middle cerebral artery
MRI	Magnetic resonance imaging
NA	Numerical aperture
Norm.	Normalized
NDB	Nucleus of the diagonal band of Broca
PMv	Ventral pre-motor cortex
PS	Post-stroke
PV	Parvalbumin
rCBV	Relative cerebral blood volume
ROI	Region of interest
rTMS	Repetitive transcranial magnetic stimulation
S	Second(s)
S1	Primary somatosensory cortex
SD	Standard deviation
SI	Skewness index
S.E.M	Standard error of means
SOM	Somatostatin
tDCS	Transcranial direct current stimulation
TIFF	Tagged image format file
V1	Primary visual cortex
vGlut1	Vesicular glutamate transporter 1

VIP	Vasoactive intestinal peptide
VSD	Voltage sensitive dye

1 _ Introduction

1.1 Stroke in the real world

Stroke is a condition in which the blood supply to the brain is disturbed and gives rise to cell death. Interruptions to blood flow that occur as a result of a blockage or clot in a vessel are referred to as ischemic strokes. Ischemic strokes account for the vast majority of strokes (>80 %). Disturbance in brain blood flow can also be the result of leakage or the rupture of a vessel, a phenomenon referred to as a hemorrhagic stroke (Heart and Stroke Foundation). Stroke is estimated to affect ~17 million people (first stroke) every year worldwide (Feigin et al., 2014). Over the past few decades, there have been considerable improvements in hyperacute and acute care (care within hours to days after stroke, respectively) provided to stroke patients which has led to a decrease in the prevalence of fatality associated with the incident (Lackland et al., 2014; Ward, 2017). Decreased mortality translates to an increase in the survival of the patients following stroke which means that, depending on the severity and the location, stroke related damage causes survivors to suffer long-term mild to severe impairments of sensory, motor and cognitive functions. These functional impairments in most cases lead to chronic disabilities and render stroke survivors dependent on others for their daily activities. Not only does this dependence lowers patients' quality of life, but it also creates a substantial economical burden on society (Ward, 2017). Following stroke, patients may experience varying degrees of spontaneous recovery that involve partial restoration of impaired functions and the development of new compensatory behaviours that result in enhanced sensory and motor performance. Spontaneous recovery is

observed from days to months following the initial insult and could be further facilitated by limited available therapeutic options like rehabilitative physical therapies (Dancause et al., 2005; Veerbeek et al., 2014). Unfortunately, in most cases, neither the spontaneous recovery nor physical therapeutic techniques guarantee the full recovery of patients, thereby demonstrating why stroke is one of the chief causes of long term disability (Veerbeek et al., 2014).

Despite considerable advances in stroke research, a mechanistic understanding of how neural circuits change when recovering from an ischemic event, is still not well understood. Accordingly, research focused on discovering the underlying mechanisms involved in stroke recovery is critical to the development of effective therapeutic interventions.

1.2 Behavioural, structural and functional adaptations following experimental cortical stroke

1.2.1 Modelling stroke in experimental animals

Development of animal models that mimic the pathophysiological features of stroke in humans has provided a means for researchers to study the mechanisms involved in brain recovery and to assess the efficacy of different treatment strategies. Currently, the most commonly used models for the study of stroke include the occlusion of major arteries, photothrombosis, and injection of vasoconstrictors (such as endothelin-1) into the parenchymal region of interest. Although occlusion of major arteries (especially middle cerebral artery or MCA and its branches) best mimics the pathological consequences of the most prevalent type of ischemic stroke in humans, it has its

limitations as an experimental model (Carmichael, 2005; Gerrow and Brown, 2017). Occlusion of major arteries normally involves invasive surgical procedures and exhibits high mortality rates. Additionally, differences in brain vascular networks across individual animals, reduce spatial control over the precise size and location of brain damage in these models, which in turn, increases the variability of behavioral deficits (Gonzalez and Kolb, 2003; Carmichael, 2005).

In 1985, Watson and his colleagues developed the photothrombotic model of stroke (Watson et al., 1985). This technique is a reliable model for inducing focal ischemic injury in discretely defined cortical regions using photoactivation of a light sensitive dye that was systematically injected into animals. This phenomenon results in an aggregation of platelets and the induction of thrombosis, which subsequently, gives rise to the occlusion of cortical vessels and an interruption of local blood circulation (Watson et al., 1985). The important advantage of the photothrombotic model over other stroke models is that it allows precise control over the size and location of the damage and results in predictable functional deficits (Carmichael, 2005). Additionally the induction of photothrombotic damage does not require invasive surgery and could be achieved by illuminating the cortical surface through the skull or a cranial window. These characteristics make this model ideal for precise assessments of stroke-induced structural and functional changes in brain networks (Jablonka et al., 2010).

1.2.2 Behavioural changes

Similar to humans, rodents that are subjected to an ischemic stroke show profound changes in their behaviour. In order to study the behavioural effects of stroke, most studies have examined sensory-motor changes in the rodent forepaw after focal

ischemic stroke in the sensory or motor cortex. In the first week after stroke, rodents show major deficits in their ability to grasp pellets, walk across a balance beam or take proper steps across a horizontal ladder. These deficits also include a seeming loss of (or reduction in) awareness of the stroke affected paw as shown when rats and mice ignore pieces of tape stuck to their paw. Interestingly, most behavioural studies report improvements in paw function within the first month of stroke recovery which usually levels off thereafter. Even though physical rehabilitation and other stroke therapies can improve the rate and magnitude of recovery (Clark, et al., 2019), most rodents will show some degree of improvement without any intervention at all.

1.2.3 Evidence for structural rewiring

Brain tissue adjacent to the infarct region, termed the peri-infarct area, has shown to play an important role in post stroke recovery. For example, disrupting the peri-infarct region with protein-synthesis inhibitors (Kim et al., 2018) or removing a portion of it (Castro-Alamanacos and Borrell, 1995) can reinstate a deficit in a behaviour that showed some degree of recovery. Based on these findings, it is thought that the recovery of sensation or movement is mediated through adaptive plasticity mechanisms in functionally related brain regions adjacent to the stroke (Carmichael et al., 2003; Dancause et al., 2005; Brown et al., 2007; Winship and Murphy, 2009).

The surviving peri-infarct neuronal networks reconstruct lost and/or damaged connections and partially assume the sensory or motor processing functions of damaged tissue (Winship and Murphy, 2009). This remodeling is manifested by structural rewiring of neuronal components that include the growth or retraction of dendritic arbors, axonal sprouting or synaptogenesis (Dancause et al., 2005; Brown et al., 2008). For example,

longitudinal *in-vivo* imaging of dendritic branches in ischemic sensorimotor cortex of mouse models has revealed that apical dendritic arbors of fully mature cortical pyramidal neurons can grow or retract dendritic tips, especially within the first two weeks after ischemic damage (Brown et al., 2010). Due to the important role of dendritic arbors in the integration of synaptic inputs (Spruston, 2008; Brown et al., 2010) this extensive remodeling could be the basis for stroke induced changes in neuronal receptive fields (Winship and Murphy, 2009) that are required for assumption of new processing functions.

Post ischemic structural rewiring has been reported in various cortical regions in different animal models of stroke. Tract tracing of ventral pre-motor (PMv) cortical connections in primate models of stroke revealed an atypical emergence of a large number of labeled terminals in forelimb somatosensory cortex (FLS1), especially in areas 1/2 of FLS1, months after cortical damage to the forelimb primary motor cortex (FLM1). The appearance of these new terminals was accompanied by changes in trajectory and orientation of PMv axonal fibers in the peri-infarct area, such that fibers that were initially directed toward FLM1 changed their trajectory towards FLS1 cortical area. These data suggest that axons from spared regions of motor cortex sprout axons towards related areas of the somatosensory cortex as a potential compensatory mechanism underlying functional recovery from a cortical injury (Dancause et al., 2005). It is important to note that structural changes after stroke are not necessarily limited to neuronal processes. Previous studies have demonstrated significant changes in other cortical components such as pericytes, astrocytes, and vascular endothelium in the peri

infarct tissue which may affect both acute and chronic stages of recovery from stroke (Nahirney et al., 2016).

1.2.4 Evidence for functional recovery

Post-stroke structural rewiring of cortical networks is associated with concomitant functional changes. Voltage sensitive dyes (VSD) are a tool commonly used to directly assess the spatiotemporal dynamics of cortical sensory processing with high temporal fidelity (Shoham et al., 1999; Brown et al., 2009). VSD imaging of mouse FLS1 cortex showed that brief stimulation of animal forepaw gave rise to a robust depolarization in the contralateral FL somatosensory areas. Sensory-evoked depolarization emanates from the center of the FLS1 shortly after stimulation, spreads to adjacent cortical areas, and decays to baseline levels within 100 ms. Brown and colleagues, documented that this pattern of cortical depolarization is mostly lost one week after a photothrombotic stroke to the FLS1 cortex, which coincided with maximal sensorimotor deficits. They further reported that after eight weeks of recovery from stroke, a new pattern of stimulus-evoked cortical activation emerged. This response pattern involved an initial depolarization in the surviving portion of FLS1, which subsequently spread to the peri-infarct area, and peaked in posterior and medial regions corresponding to M1 and HL somatosensory cortex. Similarly, assessments of sensory driven hemodynamic responses of cortex collected using Intrinsic Optical Signal (IOS) imaging in mouse models showed that forepaw induced cortical responses are almost abolished one week after a targeted photothrombotic stroke in the FL somatosensory cortex. IOS imaging also substantiated

the progressive involvement of peri-infarct tissue in processing of forelimb sensory information over weeks following stroke (Brown et al., 2009). Importantly, this functional remapping of cortical areas has been shown to be accompanied with partial restoration of lost sensorimotor functions of the forepaw (Brown et al., 2009).

Other studies using different techniques have provided additional supporting evidence of functional changes after stroke. A study by Dijkhuizen et al., (2001) used magnetic resonance imaging (MRI) to image forepaw touch induced changes of relative cerebral blood volume (rCBV) in the forelimb region of the primary somatosensory cortex after middle cerebral artery (MCA) occlusion (Dijkhuizen et al., 2001). Three days after inducing a stroke, stimulation induced changes of rCBV were lost concomitant with a decline in forepaw functions. Fourteen days after the stroke, however, animals showed improvements in their impaired forepaw functions concurrent with the appearance of significant cortical responses in the regions surrounding the infarct (Dijkhuizen et al., 2001). Collectively, these data suggest that limb dysfunction is related to post-stroke loss of brain activation and that the restitution of sensorimotor functions is associated with the emergence of a new pattern of cortical activity in the surviving perilesional tissue (Dijkhuizen et al., 2001; Brown et al., 2009; Winship and Murphy, 2009).

Thus far, most studies of stroke-related changes in brain function are limited to macroscopic remapping of cortical representations. Although these studies have significantly contributed to the understanding of stroke-induced changes in aggregate neuronal activity, they do not provide clear explanations of how these changes occur at the level of individual neurons. In 2008, Winship et al., used *in-vivo* two-photon calcium imaging in order to characterize changes in the response properties of neurons within the

forelimb and hindlimb cortical representations during a 2-8 week recovery period after ischemic damage to FLS1. Imaging of sensory-evoked calcium transients of layer 2/3 neuronal somata across primary HL and FL cortical representations in healthy mice showed that individual neurons in each somatosensory region are highly selective for processing sensory information from the corresponding limb. This specificity was disrupted after stroke, such that neurons in the FL and HL areas became responsive to sensory stimulation from different limbs, including ones ipsilateral to where neurons were imaged. This reduced neuronal selectivity was most evident in the border regions between FLS1 and HLS1 and was thought to be a transitory period preceding the development of new functional roles for these cells (Winship et al., 2008).

Despite extensive research on both functional and structural underpinnings of stroke recovery, there has yet to be a longitudinal within-subject analysis of stroke induced plasticity of neuronal activity. By longitudinally imaging and tracking the activity patterns of the exact same population of neurons in this study, our results will provide useful insights into how neuronal functionality changes in response to ischemic damage.

1.3 Role of inhibition in adult cortical plasticity

Synaptic inhibition in the cortex is predominantly induced by interneurons that release the neurotransmitter gamma-aminobutyric acid (GABA). Although cortical GABAergic neurons comprise approximately 20 % of the neuronal population, their highly ramified cellular processes and their extensive reciprocal connections with

neighbouring principal excitatory neurons allow them to exhibit precise spatiotemporal control of local excitatory networks. Based on differences including, but not limited to, morphology, electrophysiological properties, molecular features, and patterns of connectivity, GABAergic neurons are considered to be a heterogeneous population. The heterogeneity demonstrated by cortical inhibitory interneurons qualifies them to carry out a wide range of functional roles such as the maintenance of excitatory/inhibitory balance, modulation of experience-dependent plasticity, context-dependent modulation of cortical activity, and the synchronization and generation of cortical rhythms (Kato et al., 1991; Kirkwood and Bear, 1994; Fu et al., 2014, 2015; Chen et al., 2015).

Previous studies suggested that maturation of intracortical inhibition is crucial for both the onset and the closure of critical period for cortical plasticity (Huang et al., 1999; Fagiolini and Hensch, 2000; Hensch, 2005). I*n-vitro* recordings from cortical slices of adult rat visual cortex showed that tetanic stimulation of the granular layer reliably elicited LTP in layer III neurons. In contrast, delivery of tetanic stimulation to white matter failed to elicit LTP in the same cortical area unless in the presence of bicuculline methiodide (a $GABA_A$ antagonist). This observation suggested a role of intracortical inhibitory circuits referred to as “plasticity gates” in constraining the neuronal activity levels required for synaptic potentiation (Kirkwood and Bear, 1994). According to this viewpoint, many studies have attributed the maximal cortical plasticity in early postnatal periods to the immaturity of inhibitory circuits (Komatsu, 1983; Kato et al., 1991; Kirkwood and Bear, 1994).

In keeping up with these observations, Harauvoz et al., showed that reducing GABA transmission by inhibiting the activity of GABA synthetic enzyme GAD

(glutamic acid decarboxylase) or by antagonizing $GABA_A$ receptors, induced a significant ocular dominance shift in favor of the non-deprived eye which persisted even after the end of the treatment (Harauzov et al., 2010). Similarly, it was shown by Vetencourt and colleagues that chronic treatment of adult amblyopic rats with fluoxetine (an antidepressant medication) promoted the recovery of visual functions by reinstating ocular dominance plasticity (Vetencourt et al., 2008). Fluoxetine treatment led to reduced levels of GABA in visual cortex, which enabled the induction of LTP in cortical layer II/III by stimulation of white matter, a phenomenon that is normally absent in adult brain. Interestingly, intracortical infusion of benzodiazepine agonist, diazepam, prevented changes in ocular dominance in fluoxetine treated rats, suggesting the crucial role of GABA inhibition in the occurrence of adult cortical plasticity in the visual cortex (Vetencourt et al., 2008).

In recent years, there has been substantial research examining the role of inhibition in cortical plasticity during development and adulthood. These studies have approached inhibitory circuits from different angles by characterizing neurotransmitter release, receptor expression, the role of different subpopulations of inhibitory neurons and concluded that GABAergic inhibition plays an important role in the regulation of cortical plasticity (Vetencourt et al., 2008; Harauvoz et al., 2010; Fu et al., 2015; Takesian et al., 2018). Similarities between the mechanisms involved in experience dependent plasticity in the healthy brain and adaptive plasticity mechanisms that occur in the chronic stage of recovery from stroke motivated further examination of the role of inhibitory signalling in the stroke affected brain.

1.4 Role of inhibition in post-stroke cortical rewiring

Accumulating evidence suggests that inhibitory signaling is critical to the post stroke remapping of sensorimotor representations that are required for functional recovery. Ischemic damage in the cortex is accompanied by an increase in tonic GABAergic synaptic transmission in the peri-infarct region. Increased tonic inhibition mediated by extrasynaptic $GABA_A$ receptors is thought to suppress the typical recovery of cortical excitability and responsiveness after stroke. Supressing tonic inhibition by blocking α5-subunit-containing $GABA_A$ receptors or genetically reducing the number of α5- or δ-subunit-containing $GABA_A$ receptors which are involved in tonic inhibition has been shown to be beneficial to the recovery of motor functions after stroke in mice (Clarkson et al., 2010). Likewise, rats with focal ischemia that received a chronic low dosage of L-655,708 a $GABA_A$ inverse agonist with high affinity to α5 subunit, demonstrated a progressive reduction in the volumes of the necrotic core and perilesional tissue, coincident with improvements in animals performance in skilled reaching tasks (Lake et al., 2015). These studies suggest the reducing post-stroke tonic inhibition may function as a chronic treatment strategy for improving the recovery of sensorimotor functions.

On the other hand, some human case studies have documented that the treatment of stroke patients with zolpidem, a $GABA_A$ positive allosteric modulator, promotes the recovery of language, cognitive and motor functions (Crestani et al., 2000). Further, an experimental study reported that low doses of zolpidem from 3 to 28 days after MCAo or photothrombotic stroke has beneficial effects on recovery of sensory and motor abilities (Hiu et al., 2016). While a mechanistic explanation for this effect was not clear, the

authors showed that zolpidem further increases inhibitory GABA-ergic currents on layer 5 sensorimotor pyramidal neurons (Hiu et al., 2016). However, due to the complex effect of zolpidem on GABA receptors, including both tonic and phasic inhibition, these observations only imply an influential role of inhibition in post stroke recovery and do not allow for an interpretation of the underlying mechanisms.

In addition to changes in synaptic and extrasynaptic inhibition, stroke causes alterations in the expression levels of GABA receptors in the core and surroundings of the infarct region. Quantitative receptor autoradiography of brains after photothrombotic infarction revealed a long-lasting reduction of $GABA_A$ receptors in widespread brain areas ipsilateral to the lesion (Schiene, 1996). In contrast to $GABA_A$ receptors, $GABA_B$ receptors are upregulated in the perilesional and distal cortical areas of both hemispheres (Que et al., 1999). Quantitative competitive reverse transcription-polymerase chain reaction (cRT-PCR) and semi-quantitative Western blot analysis of brain tissue showed that $GABA_A$ receptor α1-subunit mRNA levels were decreased ipsilateral and contralateral to the infarct at 7 days, but were increased bilaterally at 30 days following photothrombotic brain damage in rats (Kharlamov et al., 2008). Although general consensus has not been reached regarding how the expression of GABA receptors changes following stroke, downregulation of GABA receptors could be proposed to be a homeostatic compensatory response to excessive tonic signalling after stroke.

Collectively, these studies highlight the role of inhibition in modulating brain repair and recovery from stroke. It can be concluded that recovery from stroke is accompanied by changes in neuronal excitability in the perilesional tissue and that upregulating cortical excitability (or decreasing inhibitory transmission) may facilitate

certain mechanisms underlying network plasticity that are required for the restitution of lost sensorimotor functions. In agreement with this idea, there has been supporting clinical evidence indicating that enhancing cortical excitability by external stimulation of the perilesional brain tissue may have beneficial effects on post-stroke functional recovery. Kim et al, reported that high-frequency repetitive transcranial magnetic stimulation (rTMS) of the ipsilesional motor cortex in chronic stroke patients, enhanced the excitability of corticomotor circuits and resulted in improvements in functionality of the paretic hand in a series of finger motor tasks (Kim et al., 2006). Similarly, non-invasive transcranial direct current stimulation (tDCS) of the brain has been shown to enhance the beneficial effects of rehabilitative training on brain plasticity (Nitsche et al., 2003; Butefisch et al., 2004). In 2005, Hummel and colleagues reported that delivery of tDCS to the motor cortex of the stroke affected hemisphere in patients with chronic stroke deficits resulted in functional improvements in the motor performance of every subject tested in the study. Although the exact cellular or molecular mechanisms through which cortical stimulation promotes neuroplasticity are not well understood, it has been proposed that the enhanced cortical excitability facilitates LTP-like processes required for the strengthening and maintenance of new synaptic connections after stroke (Kim et al., 2006; Fritsch et al., 2010).

1.5 Role of VIP interneurons in cortical plasticity

Although studying the role of different neuronal subpopulations in the cortex is difficult, advances in genetic tools in the past decade have allowed targeted labeling, recording, and perturbation (via optogenetics or pharmagenetics) of the *in-vivo* activity of distinct subtypes of neurons and facilitated the examination of cortical circuits including inhibitory components (Luo et al., 2018). In particular, there has been extensive recent research on the functional and anatomical characterization of cortical GABAergic neurons. This population of inhibitory neurons is comprised of three non-overlapping subpopulations that express specific markers, namely parvalbumin (PV)-, somatostatin (SOM)- and vasoactive intestinal peptide (VIP). These distinct populations of interneurons have been shown to exhibit specific structural and functional features, and play unique roles in brain circuitry.

In the context of this study, inhibitory interneurons that express vasoactive intestinal peptide are thought to play a critical role in regulating cortical excitability by suppressing the firing of other inhibitory neurons i.e. PV- and SOM-expressing subtypes that directly synapse onto peri-somatic and dendritic branches of excitatory cells, respectively (Gentet et al., 2012; Pfefferet al., 2013). VIP-expressing neurons have been reported to comprise approximately 13% of GABAergic neurons in the barrel cortex (Prönneke et al., 2015). Like other GABAergic neurons, these cells express the inhibitory marker glutamate decarboxylase (GAD). In contrast, it has been shown that they do not express, PV, SOM, or the excitatory marker vesicular glutamate transporter 1 (vGlut1) (Prönneke et al., 2015). VIP neurons mostly exhibit a bipolar morphology and are distributed across the cortex in a layer dependent manner, such that the majority of them

(~60%) are located in layer II/III with the remaining 40% of population being distributed across all other cortical layers. These neurons also show differences in their morphological and electrophysiological properties. Layer II/III VIP neurons project their dendritic branches to Layers I and II/III and their axons span all cortical layers, whereas layer IV-VI VIP neurons extend their dendritic branches throughout all cortical layers with their axons mostly restricted to layer V and VI (Prönneke et al., 2015). In particular, the axon terminals of layer II/III VIP neurons are mostly local, situated in layer II/III or layer Va/b where most of other inhibitory neurons (PV and SOM) reside (Xu et al., 2010; Prönneke et al., 2015). Electrophysiological recording from layer II/III VIP neurons in the barrel cortex showed that they exhibit great variability in their firing pattern, however the majority of these cells showed either continuous adapting (67.6%), irregular spiking (14.7 %) or bursting (11.8 %) firing patterns when depolarized (Karagiannis et al., 2009; Prönneke et al., 2015).

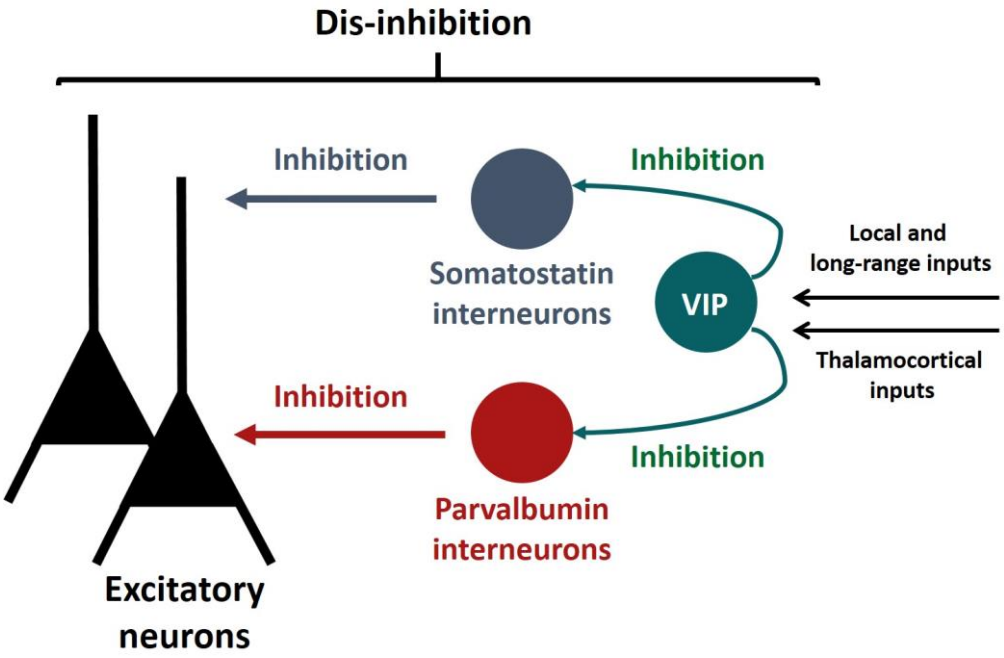

Figure 1. Schematic representation of dis-inhibitory circuit

VIP-expressing neurons project their inputs to other subtypes of inhibitory neurons. PV- and SOM-expressing subtypes synapse onto peri-somatic and dendritic branches of excitatory neurons, respectively. Essentially, activation of VIP neurons releases excitatory neurons from inhibition by PV- and SOM- expressing neurons, thereby enhancing their excitability.

VIP neurons have been shown to receive inputs from multiple sources including local excitatory neurons (Porter et al., 1998; Wall et al., 2016), thalamocortical projections from the ventral posteromedial nucleus (Staiger et al., 1996), the nucleus of the diagonal band of Broca (NDB) - a cholinergic center in basal forebrain (Fu et al., 2014) and long-range inputs from other cortical regions (Lee et al., 2013). Accordingly VIP neurons are well-designed to integrate widespread inputs from various sources,

allowing the precise regulation of functions in local excitatory networks (Wall et al., 2016).

There is now considerable evidence, from multiple cortical regions that support the idea that VIP neurons act as a dis-inhibitory circuit (Pfeffer et al., 2013; Pi et al., 2013; Lee et al., 2013; Fu et al., 2014, 2015; Jackson et al., 2016). Synchronized photo-activation of a sparse population of VIP interneurons using channelrhodopsin-2 in awake mice, resulted in significant increase in the firing rate of ~20% of cortical neurons for tens to hundreds of millisecond in the auditory and medial prefrontal cortex (Pi et al., 2013). Activation of VIP cells was followed by immediate monosynaptic inhibition of a group of neurons with spike shape and firing patterns similar to other inhibitory neurons, as well as longer latency increases in the firing rates of cells with electrophysiological features similar to excitatory cells (Pi et al., 2013). Furthermore, immunohistochemical analysis of brain tissue showed that the expression level of the neuronal activity marker "c-Fos" was significantly increased in excitatory neurons subsequent to photostimulation of VIP neurons (Pi et al., 2013).

Dis-inhibitory cortical circuits have also been shown to play an important role in sensory information processing by modulating sensory-evoked responses in a behavioural state dependent manner. Using two-photon calcium imaging of freely moving head-fixed mice, Fu et al., showed that the activity of VIP neurons in the mouse visual area (V1) is closely correlated with locomotion, and that locomotion or artificial activation of VIP neurons using optogenetics gave rise to a significant increase in sensory-evoked visual responses. Consistent with this data, they showed that photolytic damage of VIP neurons abolishes the enhancement of cortical responses by locomotion (Fu et al., 2014). A more

recent study from Jackson et al., (2016) found that both spontaneous activity in VIP neurons during resting periods or under anesthesia were highly correlated with the local increases in the activity of excitatory pyramidal neurons. Similar to the Fu et al, study, pharmacogenetic silencing of VIP neuron activity using inhibitory "Designer Receptor Exclusively Activated by Designer Drugs" (DREADDs-hM4Di) induced a reduction in local cortical activity levels during locomotion, immobility, anesthesia, and during periods of visual stimulation.

A dis-inhibitory role for VIP circuits has also been described in non-visual cortical areas. For example, it has been shown during mouse whisking, long range projections from the motor cortex synapse directly onto VIP neurons in barrel cortex which leads to a concomitant decrease in SOM interneuron activity (Lee et al, 2013). This is consistent with previous *in-vivo* observations that, VIP neurons tend to be more active during movement related behavioural states (i.e. whisking or running) that leads to the suppression of SOM expressing interneuron activity (Lee et al., 2013). The behaviourally relevant modulatory role of dis-inhibition is also reported in the enhancement of auditory cortical responses during an auditory discrimination task. In this task, VIP neurons are activated in response to reinforcement feedback signals such as reward or punishment, which then enhances the recruitment of excitatory principal neurons in the auditory response (Pi et al., 2013). Collectively, these findings show that VIP neurons are highly active during sensory-motor or sensory discrimination tasks and likely contribute to improvements in task performance by facilitating the activity of principle neurons through dis-inhibition.

More importantly, Michael Stryker and colleagues have revealed an important function of the VIP dis-inhibitory circuit in regulating adult ocular dominance plasticity. Based on their previous work showing that locomotion enhances the return of neural activity in visual cortex after monocular eye closure (and subsequent opening), they hypothesized that this enhancing effect was mediated through VIP-SOM circuit. Repeated measurements of visual responses in the binocular zone of V1 showed that silencing synaptic transmission of VIP neurons abolished the locomotion induced return of visual responses after a prolonged period of monocular deprivation. It was also shown that optogenetic activation of VIP neurons gave rise to dramatic potentiation of the visual cortical responses from the open eye after only a short 5-day period of monocular deprivation in adult mice (Fu et al., 2015). Collectively, these studies outline the influential role of VIP-expressing neurons on adult cortical plasticity and the means by which they govern the activity levels, both sensory-evoked and spontaneous, of local excitatory networks in a diverse range of brain and behavioural context.

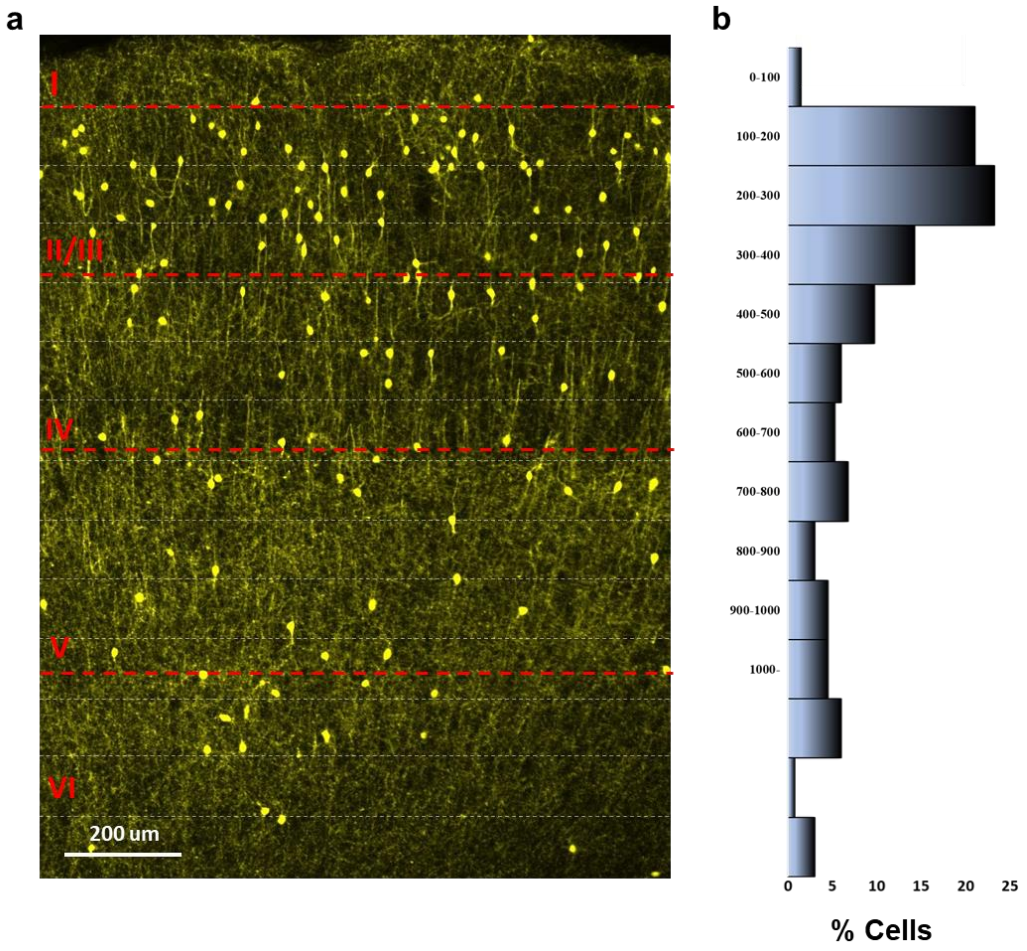

Figure 2. Distribution of fluorescently labeled somata of VIP-expressing neurons in FLS1

(a) Fluorescent image of a 50 µm thick coronal section through FLS1 of a transgenic mouse in which a Vip-IRES-cre line was crossed with an Ai9 (RCL-tdT) line (Jackson laboratory No. 007909). The Ai9 line of mice express robust tdTomato fluorescence following Cre-mediated recombination. **(b)** The distribution of Cre-expressing VIP neurons as a percentage of cells in the corresponding bins in (a) is shown on the bar graph. Cell bodies were counted in 100 µm wide bins ranging from the pial surface (0 µm) to the white matter border. Note that VIP interneurons are most populated in superficial layers.

1.6 Research rationale and objectives

Recovery from stroke requires functional and structural remapping of lost or damaged sensorimotor circuits in the surviving peri-infarct tissue. Previous studies have demonstrated that ischemic brain damage leads to decreased cortical responsiveness to sensory stimuli in the stroke affected hemisphere. Lack of cortical responsiveness (defined at both a cellular and regional level), especially with one week after the stroke, coincides with the period of maximal sensorimotor deficits. Ongoing recovery after stroke is accompanied by the return of cortical responsiveness to sensory stimuli in the surviving peri-infarct regions, and that correlates with improvements in sensorimotor performance. Based on the existing literature, it is conceivable that stroke related changes in cortical excitability may be governed by concomitant changes in the activity of inhibitory circuits. Dis-inhibitory VIP interneurons govern the activity of local excitatory networks by supressing the activity of other inhibitory neurons (i.e. PV- and SOM-expressing subtypes that directly synapse onto peri-somatic and dendritic branches of excitatory cells respectively). VIP neurons have also been shown to play important roles in sensory processing as they enhance the amplitude of sensory-evoked cortical responses in excitatory neurons (Pfeffer et al., 2013; Pi et al., 2013; Lee et al., 2013; Fu et al., 2014; Jackson et al., 2016). Accordingly, it is conceivable that stroke related changes to VIP neuron activity/excitability in somatosensory cortex could help explain why cortical network excitability is suppressed after stroke. Unfortunately, there has not been a single study that has characterized the activity or excitability of VIP neurons after stroke. Therefore, I explored the consequences of ischemic damage to the functionality of these interneurons in a mouse model of stroke. I performed longitudinal two-photon calcium

imaging and followed the activity of the exact same population of VIP neurons before, and until 4-5 weeks after, a photothrombotic insult to the cortex *in-vivo*.

Investigating the functionality of different subtypes of neurons is important not only for obtaining a clearer understanding of how the brain processes information following stroke, but also for providing potential therapeutic target sites for artificial modulation of cortical activity.

1.7 Imaging VIP neuron activity using GCaMP6s

GCaMP6s is a genetically encoded calcium indicator (GECI) created by fusion of circularly permuted green fluorescent protein, the calcium-binding protein calmodulin and Calmodulin-interacting M13 peptide (Chen et al., 2013). This protein can be delivered to specific cell types or subcellular compartments and used as a sensor for monitoring intracellular calcium dynamics. Essentially, binding of calcium ions to the calmodulin domain of GCaMP6s results in a conformational change in calmodulin and subsequently M13 domains. These calcium-dependent conformational changes, includes modulation of solvent access and the pKa of the chromophore, which leads to an increase in the brightness of cpGFP (Chen et al., 2013). Importantly, due to the tight coupling of neuronal activity and changes in intercellular free calcium, GECIs including GCaMP6s are powerful means to monitor and image the activity of designated neuronal populations in a minimally invasive manner.

2 _ Methods

2.1 Animals

Two- to five-month-old male VIP-cre mice (Vip-IRES-cre, obtained from Jackson Laboratory, stock no. 010908) were used in this study. Mice were housed in groups of 2-5 under a 12 hours light/dark cycle and given access to ad libitum water and food. All experiments were conducted in accordance with the guidelines laid out by the Canadian Council of Animal Care and approved by the University of Victoria Animal Care Committee.

2.2 AAV injections and cranial window surgery

Mice were anesthetized with isoflurane (2% induction, 1.5% maintenance) mixed in medical air and fitted into a custom-made surgical stage. An ophthalmic liquid gel was applied on the eyes to avoid dryness. During the procedure, animals were kept on a heating pad and their body temperature was maintained at 37°C, using a rectal thermo-probe and a temperature feedback regulator. Animals received 0.03 ml injection of dexamethasone subcutaneously to reduce any surgery-induced inflammation during and after the procedure. A magnetic metal ring (outer diameter 11.3 mm, inner 7.0 mm, height 1.5 mm) was secured to the skull (cyanoacrylate glue) centered on the FL somatosensory cortex (2.5 mm lateral to bregma). Using a high speed drill, a small hole was drilled through the skull for AAV injections. 600 nl volume of virus solution containing 1:30 dilution of AAV.Syn.Flex.GCaMP6s (University of Pennsylvania Vector Core) was injected to the cortex. Injections were done using a glass micropipette with the tip diameter of ~30-50 µm connected to a Hamilton syringe.

Following AAV injection, a 4 mm diameter craniotomy was drilled in the center of metal ring. Cold HEPES-buffered artificial cerebrospinal fluid (ACSF) was intermittently applied to the skull during the drilling procedure to keep the brain moist and cool. The thinned portion of skull bone was removed (leaving the dura intact) and was covered with a circular glass coverslip (no.1 thickness). The coverslip was affixed to the skull using cyanoacrylate glue and dental cement. Following AAV injection and cranial window implantation, mice were allowed to recover from anesthesia under a heat lamp and transferred to their home cage. After four weeks of recovery from the surgery, the quality of imaging windows was examined and windows with a significant loss of clarity were excluded from the study.

2.3 Intrinsic optical signal (IOS) imaging

IOS imaging was performed four weeks after cranial window implantation to map cortical areas corresponding to FL and HL somatosensory cortex. The cortical surface of lightly anesthetized mice (1% isoflurane) was illuminated by a red LED (635 nm). Sensory-evoked changes in the reflectance of red light (attributable to changes in the levels of deoxy-hemoglobin and presumably neuronal activity) were collected with a MiCAM02 CCD camera (SciMedia) mounted on an upright microscope through a 2X objective. Of note that, throughout imaging, the objective plane of focus was set just below brain's surface to minimize the contribution of hemodynamic signals from large surface vessels. In order to evoke cortical responses, 1 s of vibro-tactile stimulation (5 ms bi-phasic pulses vibrating at 100 Hz) was applied to the contralateral FL or HL through a pencil lead connected to a piezo-electric element. Each imaging session consisted of

twelve stimulation/no stimulation trials with a 10 s interval between each trial. In each trial, intrinsic signals from the cortical surface were recorded over 3 s (1 s of pre- and 2 s post-stimulation) at 100 Hz, with 10ms exposure time. Twelve trials were then mean filtered (3 pixels radius) and averaged together to generate an average stack. Relative changes in reflectance of red light resulting from the stimulation ($\Delta R/Ro$) were then calculated by normalizing all images to an average intensity projection of pre-stimulus images. Subsequently, an average intensity projection of images during the post-stimulus response (0.5-2 s post-stimulus) was taken. This average response image was then thresholded (at 75% of maximum intensity) and used to superimpose the IOS map of FL and HL somatosensory areas on an image of the cortical surface vasculature.

2.4 Targeted stroke in forelimb somatosensory cortex

One day after the final pre-stroke 2-photon imaging session, a unilateral photothrombotic stroke was targeted to the forelimb somatosensory cortex in the right hemisphere through the cranial window (Watson et al., 1985). Briefly, mice were anesthetized using isoflurane (2% induction; 1.5% maintenance) mixed with medical air and placed under an Olympus BX51WI microscope. Body temperature was maintained at 37°C. Animals received an i.p injection of 1% Rose Bengal solution (100 mg/kg in HEPES-buffered ACSF). A ~1mm diameter area of the FL somatosensory cortex (using maps acquired from IOS imaging) was illuminated with a green LED (~20mW) through a 10x objective lens for 15-20 min until surface vessels had clearly stopped flowing. The infarct region was positioned in close proximity (~100 - 200 μm) to previously defined pre-stroke imaging areas. Sham stroke control mice received either Rose Bengal injection

(without illumination of green light) or illumination of green light (without the injection of photosensitive dye).

2.5 Laser speckle imaging

The cortical surface of anesthetized mice was illuminated with a 785 nm elliptical laser beam 2.4*3.4 mm coupled to a 3X beam expander (ThorLabs Inc; 1–3 mW output power). Twelve-bit images were collected with a CCD camera mounted on an Olympus microscope through a 2X objective (696*520 pixel). Imaging was performed one week post stroke. Each imaging trial consisted of 100 consecutive frames of laser speckle images (exposure time T=10 ms) of the cortical surface. Imaging trials (sequence of images) were saved as a TIFF file for further assessments.

Analysis of spatial speckle contrast was done using Imagej software. Sequence of images in each trial was averaged in order to create an average image of raw speckles. The original stack of raw speckle images were processed with a two-dimensional variance filter (3 * 3 radius) to create images of variance. Subsequently, images of standard deviation were created by taking the square root of images of variance. Images of standard deviation in each stack were averaged together and divided by the average image of raw speckles (AVG SD/AVG Mean) in order to create a speckle contrast image. This image provides a visual representation of relative blood perfusion over the brain surface where speckle contrast is inversely related to blood flow (lower pixel values corresponding to higher blood flow and higher pixel values corresponding to lower blood flow). Speckle contrast images were thresholded to 80% of maximum intensity in the infarct region. The infarct region was subsequently enclosed by a circular ROI and

mapped onto an image of the cortical surface. The distance of each area relative to the infarct border was calculated as a straight line segment from the center of area to the infarct's circular border.

2.6 Two photon *in-vivo* imaging

One week after mapping cortical representations of FL and HL somatosensory cortex using IOS images, we started pre-stroke two-photon imaging sessions to examine the response properties of GCaMP6s-expressing VIP cells. Mice were lightly anesthetized with isoflurane (2% induction, 1.0% maintenance) mixed in medical air and fitted into a custom-made imaging stage that allowed the head to be fixed under the objective. During imaging, mice were kept on a heating pad and their body temperature was maintained at 37°C. Two photon images of fluorescently labeled VIP neurons were acquired through the cranial window using an Olympus FV1000MPE laser scanning microscope equipped with a mode locked Ti:sapphire laser. Images were collected through a 20x Olympus XLUPlanFl water-immersion objective lens (NA = 0.95) at a zoom of 2x covering a 317.331 × 317.331 µm field of view (512 × 512 pixels, 0.619 µm / pixel) using Olympus Fluoview FV10-ASW software. Calcium imaging of GCaMP6s-labeled cells was performed at 4Hz with the laser tuned at a wavelength of 940 nm. Laser power delivered ranged from 20 to 60 mW at the back aperture depending on imaging depth. Emitted light was separated by a dichroic filter (552 nm) and then directed through a band pass filter (495-540nm).

Responsiveness of VIP neurons was assessed by imaging sensory-evoked calcium transients of GCaMP6s expressing cell bodies in response to 1.5 s of vibro-tactile

stimulation. Simulation was delivered to the dorsal surface of contralateral forepaw through a pencil lead connected to a piezoelectric bending actuator (Piezo Systems, Q220-A4-203YB; B300 mm deflection). “Low-intensity” or “high-intensity” vibro-tactile stimuli were delivered at 100 Hz (5 ms pulse width and 10 ms interpulse interval), which equated to providing sensory stimulation with 1mm or 4mm of lateral deflection of the stimulating element (tip of the vibrating pencil lead while not connected to the limb), respectively. Sensory-evoked calcium responses were recorded for 8 low or high intensity stimulation trials for each imaging area (trials were recorded iteratively with one minute interval between them). Images for each trial were collected at 4Hz with 5 s of pre-stimulus and 7 s of post-stimulus data acquisition.

Imaging of spontaneous activity patterns in VIP neurons within each imaging area (same cells as above) was also performed. Spontaneous calcium transients from individual cell bodies in each area were recorded at 4Hz over a 75 s period of time in the absence of any sensory stimulation.

2.7 Imaging analysis

2.7.1 Analysis of sensory-evoked responses

Individual trials were corrected for misalignments in x-y plane (possible drifts in brain position that occur during *in-vivo* imaging) using automated plug-ins StackReg and TurboReg in ImageJ software (Thevenaz et al., 1998). All images were registered to the first imaging trial. In order to define cell bodies for analysis, eight low or high intensity stimulus trials were averaged together for each imaging area. GCaMP6s expressing cell bodies were identified from an average intensity projection of the average stack. Regions of interests (ROIs) were manually drawn around each cell body in each imaging trial and

raw calcium signals were extracted by averaging all the pixels within each ROI. Raw calcium transients were adjusted for potential signal contamination emanating from labeled neuropil. The neuropil signal $F_{neuropil}$ (t) surrounding each cell was measured by averaging the signal of all pixels within a circular doughnut-shaped band, 10 μm wide, around the cell body excluding its processes and neighboring cells. The fluorescence signal of a cell body was estimated as $F_{cell\text{-}true}$ (t) = $F_{cell\text{-}measured}$ (t) – r × $F_{neuropil}$ (t) where t is time and r is the contamination ratio estimated as 0.7 for 0.95 numerical aperture (Kerlin et al., 2010; Chen et al., 2013; Dana et al., 2014; Velez et al., 2017). Neuropil corrected forelimb-evoked calcium transients in each trial ($F_{cell\text{-}true}$ or "F") were subtracted and normalized to their pre-stimulus signal ("Fo") to generate a ΔF/Fo {(F-Fo)/Fo} where Fo was the median value of fluorescent signal over 5 s before stimulation. Calcium transients for each trial were identified to be forepaw responsive if they demonstrated both: a) significant stimulus related changes in fluorescence based on a 2-tailed student t-test assuming unequal variances comparing 2.5 s following stimulus to 2.5 s preceding stimulus and b) that were at least 10% greater than pre-stimulus values (ΔF/Fo > 0.1 within 2.5s after stim). Forepaw responsive cells were subsequently defined as cells with more than one responsive trial. Given the longitudinal nature of this imaging study, cells that were not identifiable over weeks were eliminated from the analysis. Additionally, cell bodies that were not at least 5% brighter than their neuropil (based on median value of soma vs surround neuropil) were not included in the analysis. Neuronal responsiveness was evaluated by comparing the fraction of responsive cells, fraction of responsive trials and average response amplitude (ΔF/Fo).

2.7.2 Analysis of spontaneous activity

Similar to the analysis of sensory-evoked responses, spontaneous calcium traces were extracted from each cell body and corrected for potential neuropil contamination. ΔF/Fo was calculated for each calcium trace where Fo was set to be the 30^{th} percentile value of each individual trace. The standard deviation of all data points smaller than the 30^{th} percentile value of each trace was calculated ($SD_{not\text{-}event\text{-}related}$). In each calcium trace, data points that exceeded 10% of Fo value and were significantly different from not-event-related data points ($> Fo+2SD_{not\text{-}event\text{-}related}$) were considered a spontaneous calcium event. Only data points that persisted to meet the aforementioned criteria for at least six imaging frames (1.5 s), given the slow decay of GCaMP6s signals, were considered to be event related. Otherwise, they were assumed to be noise-like signal fluctuations. Subsequently, the total number of individual events and the total time associated with all calcium events in each recording were calculated and used as a measure of spontaneous activity.

2.7.3 Skewness index

In order to quantify changes in the fidelity of VIP neuron responses to sensory stimulation over time, a Skewness Index (SI) was calculated as SI : [(F0-F8) + 0.75 × (F1-F7) + 0.5 × (F2-F6) + 0.25 × (F3-F5) + N] / (2×N) where N was the total number of cells and Fx was the number of cells corresponding to X number of responsive trials (Sugiyama et al., 2008).

2.7.4 Variances of response fidelity

In order to acquire an estimate for the robustness of response fidelity between weekly imaging sessions, variances in the number of responsive trials over four post-stroke imaging sessions (PS1-PS4) were calculated for each individual cell and these

values were compared with those of the control group (week1-week4). Additionally, predictability of response fidelity was examined by calculating the squared differences of the number of responsive trials during each week's imaging session from those values collected during the preceding week's imaging session for each individual cell. These squared differences were then compared between stroke and control groups (PS1-PS5 for stroke group; week1-week4 for control group).

2.8 Statistics

Statistical analysis of the data was conducted using GraphPad Prism 8 software. Data presented in graphs are means ± standard error of the mean S.E.M. In graphs, where a comparison between groups (stroke vs control) over time was needed, a repeated measures two-way analysis of variances (ANOVA) was used to identify significant differences between groups, over time and group by time interactions. The analysis was followed up by *post-hoc* t-tests (Bonferroni's multiple comparisons test) to identify group differences at each time points. In cases where comparison between different time-points of one group were needed, a repeated measures one-way ANOVA and *post-hoc* t-tests (Dunnett's multiple comparisons test) were used to test significance. In cases where a comparison between two groups (stroke vs control) was needed, an unpaired student t-test was used to identify significant differences. P-values <0.05 were considered significant for all tests. * indicates significant comparisons (* $P<0.05$; ** $P<0.01$; *** $P<0.001$).

3 _ Result

3.1 VIP - expressing neurons are less responsive following stroke

The first goal in our study was to understand how the responses of VIP-expressing neurons changed following a targeted ischemic insult to the forelimb (FL) somatosensory (S1) cortex. To answer this question we performed longitudinal *in-vivo* two-photon calcium imaging and assessed sensory-evoked responses in these neurons. Figure 3a shows the experimental timeline used for these experiments. Seven weeks before stroke induction, VIP-IRES-Cre mice were injected with a Cre-dependant AAV to drive GCaMP6s expression (AAV1.synapsin.FLEX.GCaMP6s) in VIP neurons directly within and adjacent to the FL somatosensory cortex. At the time of AAV injection, animals were implanted with cranial windows over the right somatosensory cortex. Post-mortem examination of mice confirmed robust expression of GCaMP6s in VIP neurons, primarily in superficial cortical layers (layer I, II). As a guide for stroke and calcium imaging experiments, we mapped the macroscopic functional representations of FL and hindlimb (HL) somatosensory cortex, by imaging sensory-evoked intrinsic optical signals (IOS) from the brain surface. Mechanical stimulation of the contralateral FL or HL resulted in lower reflectance of red light from a specific region of the brain surface (Fig. 3c). This decreased reflectance is indicative of a local increase in the levels of deoxy-hemoglobin which absorb red light and presumably, demonstrates enhanced neuronal activity in that region of the brain (Frostig et al., 1990). Given the importance of the peri-infarct cortical region in assuming functional roles disrupted by ischemia, imaging of GCaMP6s in VIP neurons was mostly restricted to regions in close proximity to the infarct region (<400 µm; Fig. 3d, Fig. 6a, b).

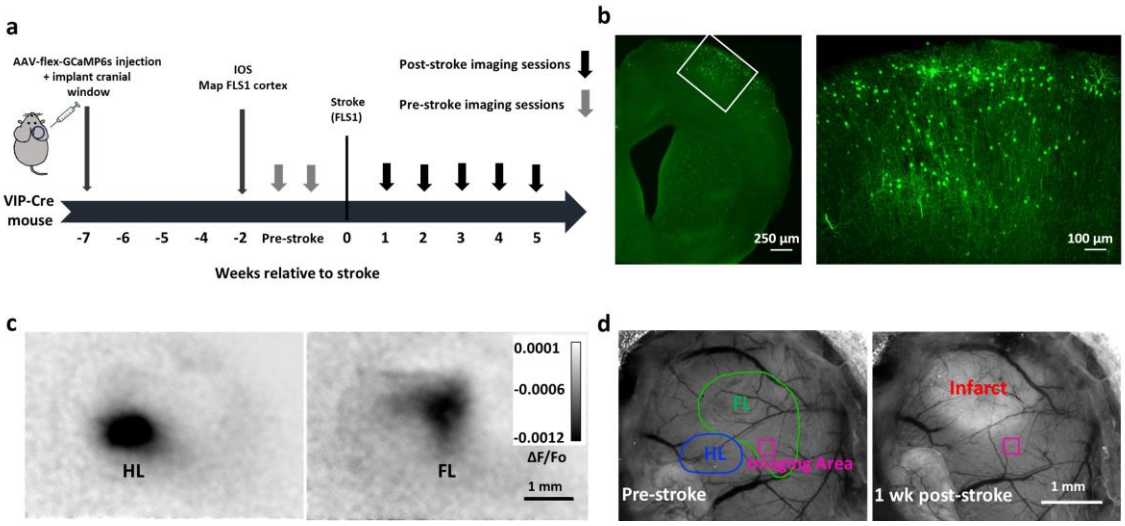

Figure 3. Graphical summary of experimental procedure, GCaMP6s expression, IOS imaging and stroke induction

(a) Experimental timeline of viral injection, IOS imaging, stroke induction and two-photon imaging. **(b)** Left, example image showing the expression of GCaMP6s in VIP neurons (no stroke) – scale bar 250 µm. Right, magnified image of the area enclosed with white box – scale bar 100 µm. **(c)** IOS imaging was used to map the cortical representations of HL (left) and FL (right) areas as a guide for stroke and calcium imaging experiments - scale bar 1mm. **(d)** Bright-field images of cortical surface before and one week after photothrombotic ischemic damage. Maps of FL and HL cortical representations from IOS imaging are delineated by green and blue lines, respectively. Size and location of one example imaging area is presented by a purple square - scale bar 1mm.

Two-photon imaging was performed weekly which allowed us to follow functional changes of the exact same population of cells before, and up to five weeks after ischemia. We imaged somatic calcium transients in response to eight trials of vibro-tactile stimulation (1.5s duration at a frequency of 100 Hz) of the contralateral forelimb (Fig 4a). The FL was stimulated using a "high" and "low" intensity vibrotactile stimulus, which equated to a 1 or 4 mm deflection of the stimulating piezo element, respectively. We reasoned that different stimulation intensities would enhance our ability to detect stroke related deficits in the response properties of VIP neurons. As shown in Figure 4b-d, sensory-evoked calcium transients were reliably detected on a trial by trial basis in a fraction of VIP neurons. Before the induction of stroke, approximately 50-60% of VIP neurons were responsive to both low and high intensity FL stimulation (see "pre-stroke" in Fig 4d,e and 5a,b-left panel), with a detectable somatic calcium transient occurring in ~50% of trials (Fig. 5a,b-middle panel). One week after stroke, there was a significant reduction in the percentage of FL responsive cells (Fig. 4d,e and 5a,b) with a ~60% reduction in the low-intensity stimulation group verses ~30% in the high-intensity group. The percentage of responsive trials (~38% in the low-intensity group; ~25% in the high-intensity group), and average response amplitude (Fig 5a,b-right panel) was also reduced in the first week after stroke. The stroke related decrease in VIP neuron responsiveness (fraction of responsive cells or trials) was more evident when animals received lower, rather than higher-intensity sensory stimulation (compare data in Fig. 5a vs. 5b). From 1 to 2 weeks recovery, the % of responsive cells and trials increased, but did not undergo further improvement in the ensuing weeks (Fig. 5a,b). It is worth noting that the fraction of responsive cells and trials were generally stable over the entire imaging period for

sham stroke control animals (Fig. 5a,b), thereby ruling out the possibility that degradation of imaging conditions over time could explain these stroke related effects on VIP neuron responsiveness. Furthermore, given the possibility that a systematic increase in normalized pre-stimulation ("resting") somatic calcium fluorescence (Fo) could influence the amplitude of sensory evoked responses and responsive trials, we compared Fo values in stroke and sham conditions, as well as correlated response amplitudes with Fo values. As shown in Figure 5c, stroke led to a reduction in Fo values that was evident at 1 week but not at later weeks. However, there was no systematic relationship between resting Fo calcium levels and the amplitude of evoked responses (Fig. 5d) or fraction of responsive trials (Fig. 5e), arguing against the idea that reduction in neural responsiveness after stroke is an artifact of changes in resting calcium levels. Collectively, these experiments and analysis indicate that stroke disrupts the responsiveness of VIP neurons to sensory stimulation.

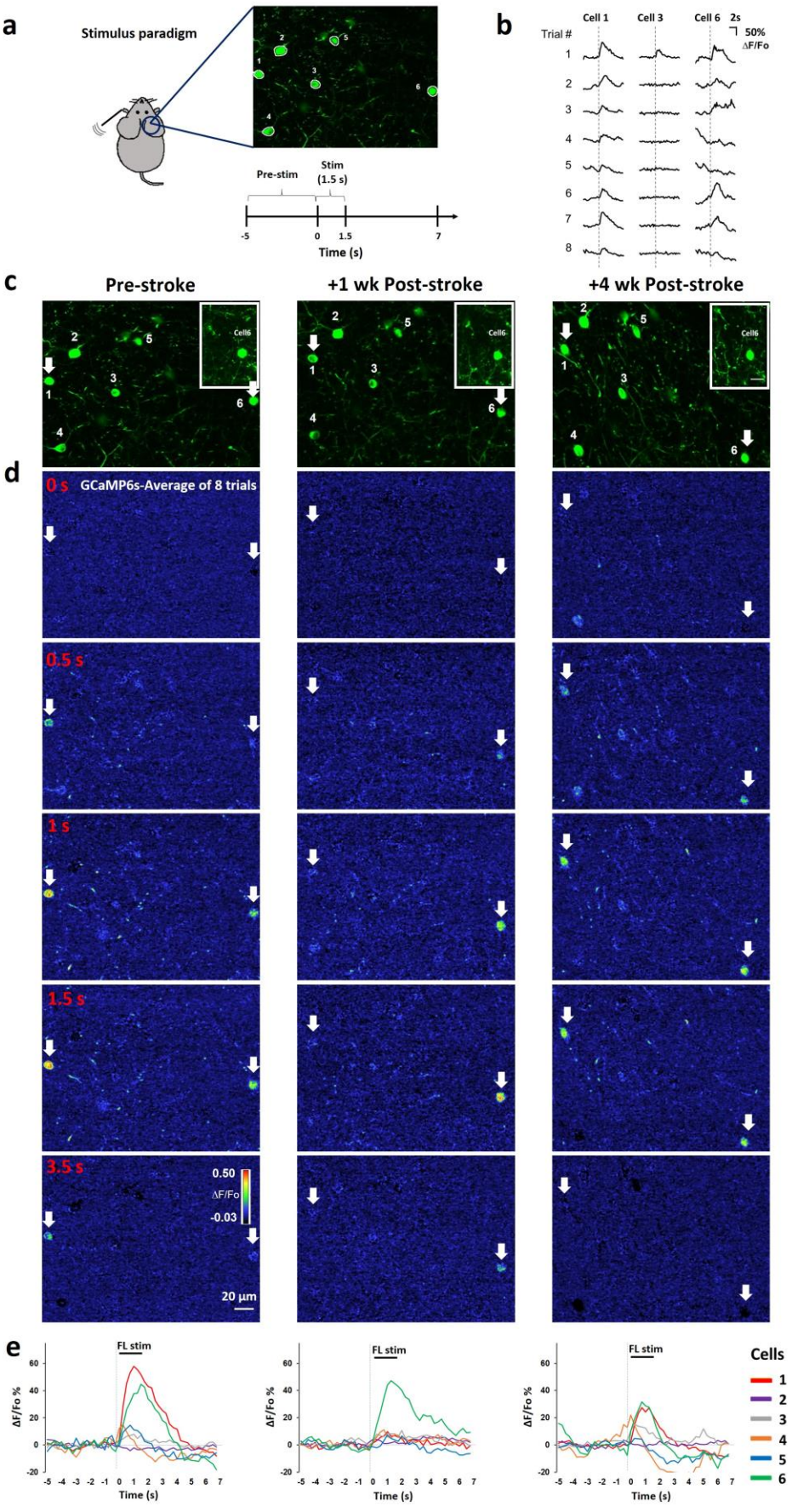
a
Stimulus paradigm
Pre-stim
Stim
(1.5 s)
-5
0
1.5
7
Time (s)
b
Cell 1
Cell 3
Cell 6
2s
50%
ΔF/Fo
Trial #
c
Pre-stroke
+1 wk Post-stroke
+4 wk Post-stroke
Cell6
d
0 s
GCaMP6s-Average of 8 trials
0.5 s
1 s
1.5 s
3.5 s
0.50
ΔF/Fo
-0.03
20 µm
e
FL stim
ΔF/Fo %
Time (s)
Cells
1
2
3
4
5
6

Figure 4. Sensory-evoked calcium (GCaMP6s) responses of VIP neurons before and after stroke

(a) Graphical summary of stimulus paradigm for each imaging trial. Somatic calcium transients in response to eight trials of vibro-tactile stimulation (1.5s duration at a frequency of 100 Hz) of the contralateral forelimb were recorded for each area **(b)** Example of individual forelimb-evoked traces (ΔF/Fo %) for three cells in (a). **(c)** Images showing the exact same population of GCaMP6s-expressing VIP neurons (numbered 1-6) in an example imaging area before stroke and at different time-points afterwards; Magnified images of Cell6 and its surrounding neuropil is displayed on top corner of each image (white box). **(d)** Colour montages show forelimb-evoked changes (averaged over 8 trials) in GCaMP6s fluorescence (ΔF/Fo) for neurons in (c) before stroke and 1-4 weeks later. Scale bar, 20 μm. **(e)** Changes in GCaMP6s fluorescence (ΔF/Fo %) from each cell body in (d) is plotted over time.

a **Low intensity stimulation**

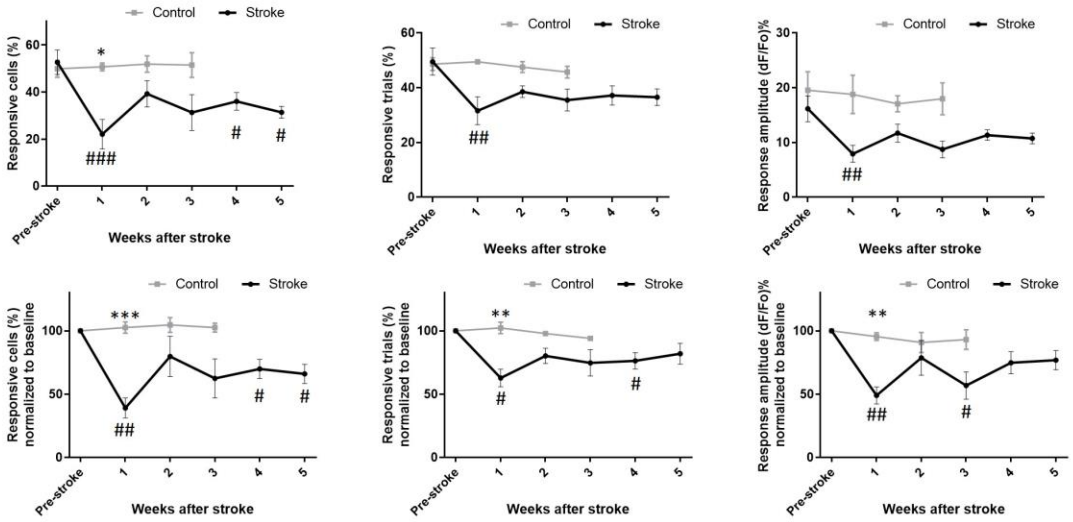

b **High intensity stimulation**

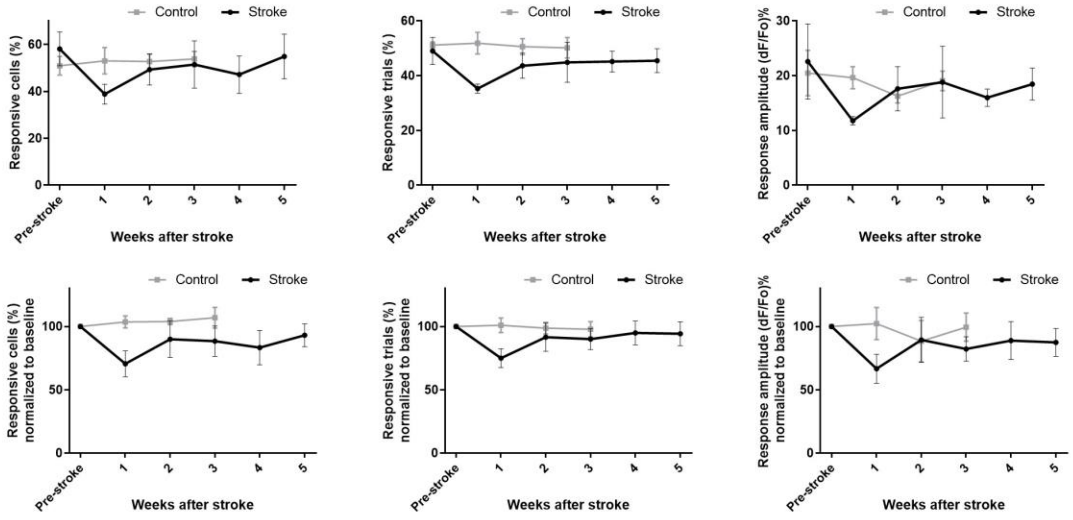

c

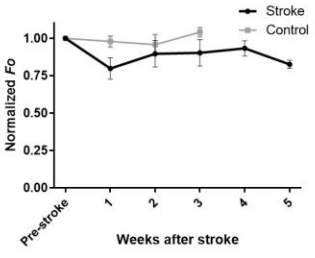

d

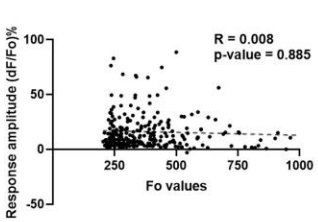

e

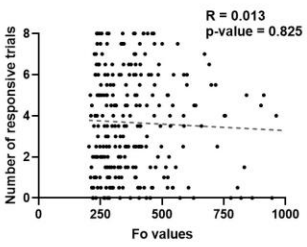

Figure 5. VIP neurons are less responsive to limb stimulation after stroke

(a) Assessment of sensory-evoked neuronal responses to "Low-intensity" stimulation of the contralateral limb. Top, the percentage of responsive cells, trials, and average response amplitude ΔF/Fo% plotted as a function of time after stroke (154 cells in 6 stroke mice; 116 cells in 4 control mice). Bottom, data in top (a) normalized to their pre-stroke levels. **(b)** Assessment of sensory-evoked neuronal responses to "High-intensity" stimulation of contralateral limb. Top, the percentage of limb responsive cells, trials and average response amplitude ΔF/Fo% plotted as a function of time after stroke (154 cells in 6 stroke mice; 116 cells in 4 control mice). Bottom, data in top (b) normalized to their pre-stroke levels**. (c-e)** Normalized GCaMP6s fluorescence (Fo) in neuronal cell bodies over time (154 cells in 6 stroke mice; 116 cells in 4 control mice). No correlation was determined between Fo values and response amplitude ΔF/Fo % (d) or the number of responsive trials (e) across the population of cells. Data are means ± S.E.M. All cells analyzed were in close proximity to the infarct region (<400 μm). * P<0.05; ** P<0.01; *** P<0.001 based on two-way ANOVA comparing stroke versus control at each time-point. # P<0.05; ## P<0.01; ### P<0.001 based on one-way ANOVA comparing post-stroke time-points in each graph relative to pre-stroke values.

3.2 Reduction in sensory-evoked responsiveness is correlated with distance from the infarct

Although most of our imaging was collected within the peri-infarct region (<400μm from infarct), more distant areas were also sampled thereby allowing us to examine how VIP neuron responses change as a function of distance from the infarct border. Therefore, we utilized laser speckle contrast imaging (LSCI) to map the distribution of flowing blood vessels on the cortical surface and calculated the distance from the center of each imaged area to the border of infarction (Fig. 6a). Changes in responsiveness of VIP neurons in each area were quantified as the fraction of responsive cells/trials at one week post-stroke relative to the fraction of responsive cells/trials at pre-stroke imaging session. These relative changes were subsequently plotted against the distance of the corresponding area from the infarct border. As is shown in Figure 6b, there is a significant correlation between the levels of post-ischemic sensory-evoked neuronal responsiveness and the distance from the infarct region. Specifically, the stroke-related decrease in neuronal response properties is primarily restricted to areas located within a close proximity to the infarct border (~400 μm). It should be noted that, these findings are consistent, and possibly associated, with other distance-related changes in synaptic structures e.g. axonal sprouting/retraction, synaptogenesis and changes in dendritic spines/bouton turnover rates that have been observed within a close proximity to the infarct border (Stroemer et al., 1995; Xerri et al., 1998; Biernaskie and Corbett, 2001; Carmichael et al., 2001; Carmichael, 2003; Gonzalez and Kolb, 2003; Brown et al., 2007).

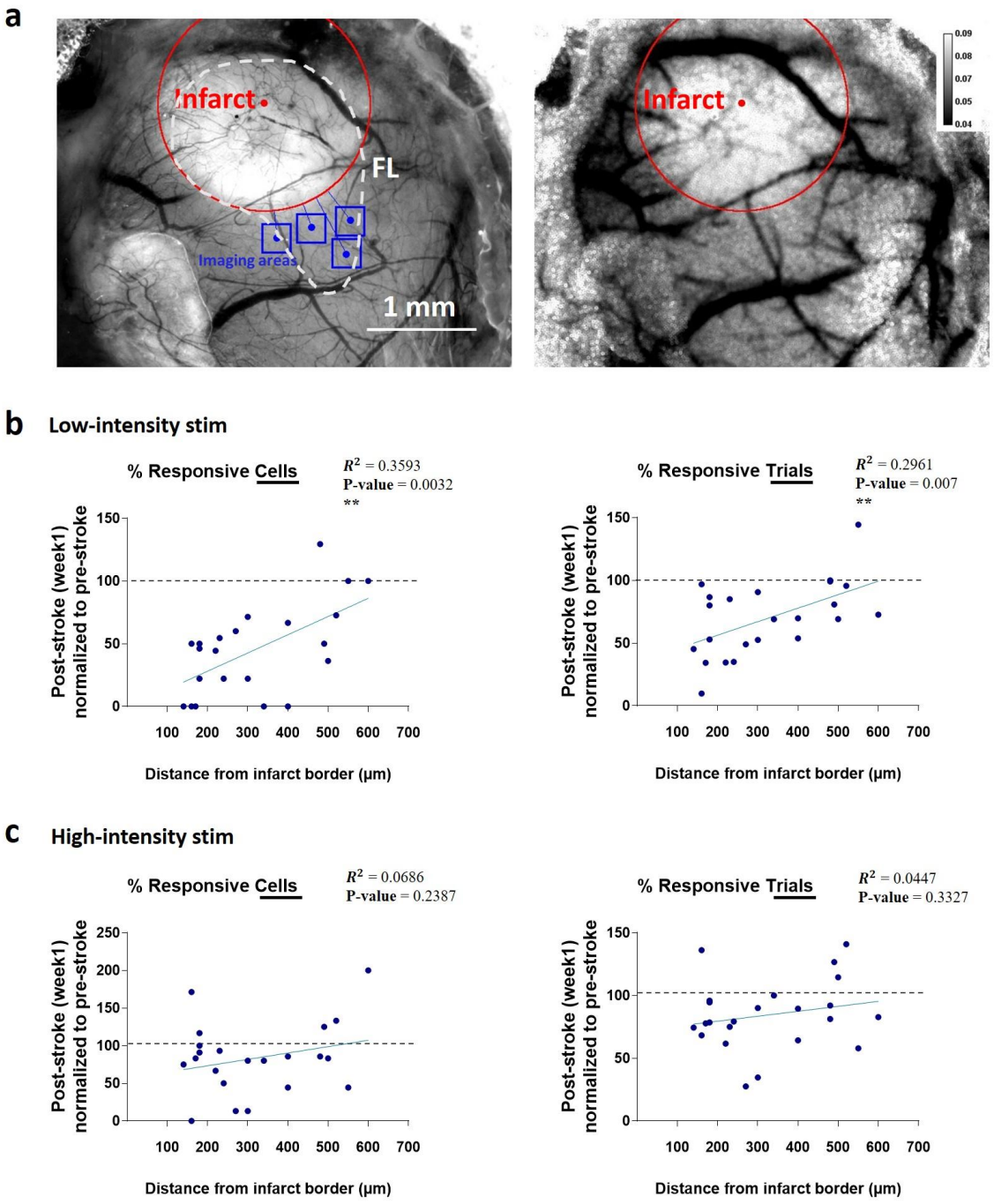

Figure 6. Reduction in sensory-evoked responsiveness is correlated with distance from the infarct border

(a) Left, an example bright field image of the brain surface showing the location of imaging areas relative to infarct boundaries (distance of each area relative to the infarct

border was measured as the length of the line segment initiating from the center of area and terminating perpendicular to the infarct's circular border). Red circle, blue boxes, and white dashed line show the infarct region, calcium imaging areas, and the relative location of FLS1, respectively. Right, laser speckle contrast image at one week post-stroke show disruption of blood flow in the infarct area (pixel values closer to 0 reflect increased blood flow). **(b-c)** Percentage of responsive cells (left) and percentage of responsive trials (right) at one week post-stroke (normalized to pre-stroke values) are shown for each imaging area and plotted against the distance of that area from the infarct boundaries. Data in **(b)** and **(c)** correspond to sensory-evoked responses to "Low-intensity" and "High-intensity" stimulation, respectively.

3.3 Effect of stroke on VIP neuron response fidelity

Given that we recorded calcium transients across eight low and high intensity stimulus trials for each peri-infarct neuron, we next asked whether stroke influences the fidelity of sensory evoked-responses (defined as a cell's number of responsive trials out of eight trials at a certain imaging week) over time. Figure 7a and b shows the frequency distribution of VIP neurons (peri-infarct area, <400μm) plotted against the corresponding number of responsive trials at different imaging time-points. At pre-stroke for both low and high intensity stimulation (Fig. 7a and b, respectively), the frequency distribution appears Gaussian with a median of 4 responsive trials and mean of 3.6 and 3.8 for low and high intensity stimulation respectively. Within one week after stroke, this distribution shifted left-ward, indicating that the majority of neurons were responsive to fewer stimulation trials (Fig. 7a,b). Over the ensuing weeks of stroke recovery, the frequency distribution shifted slightly to the right indicative of more neurons with a higher response fidelity. In order to quantify these shifts in frequency distribution, we calculated a "Skewness Index" typically used to estimate ocular dominance changes (Sugiyama, et al.

2008) (*see methods*). Based on this metric (Fig. 7c, d), VIP neuron response fidelity is significantly skewed to a lower fidelity one week after stroke that shows some, albeit minor reduction in skewness from weeks 2-5 post-stroke.

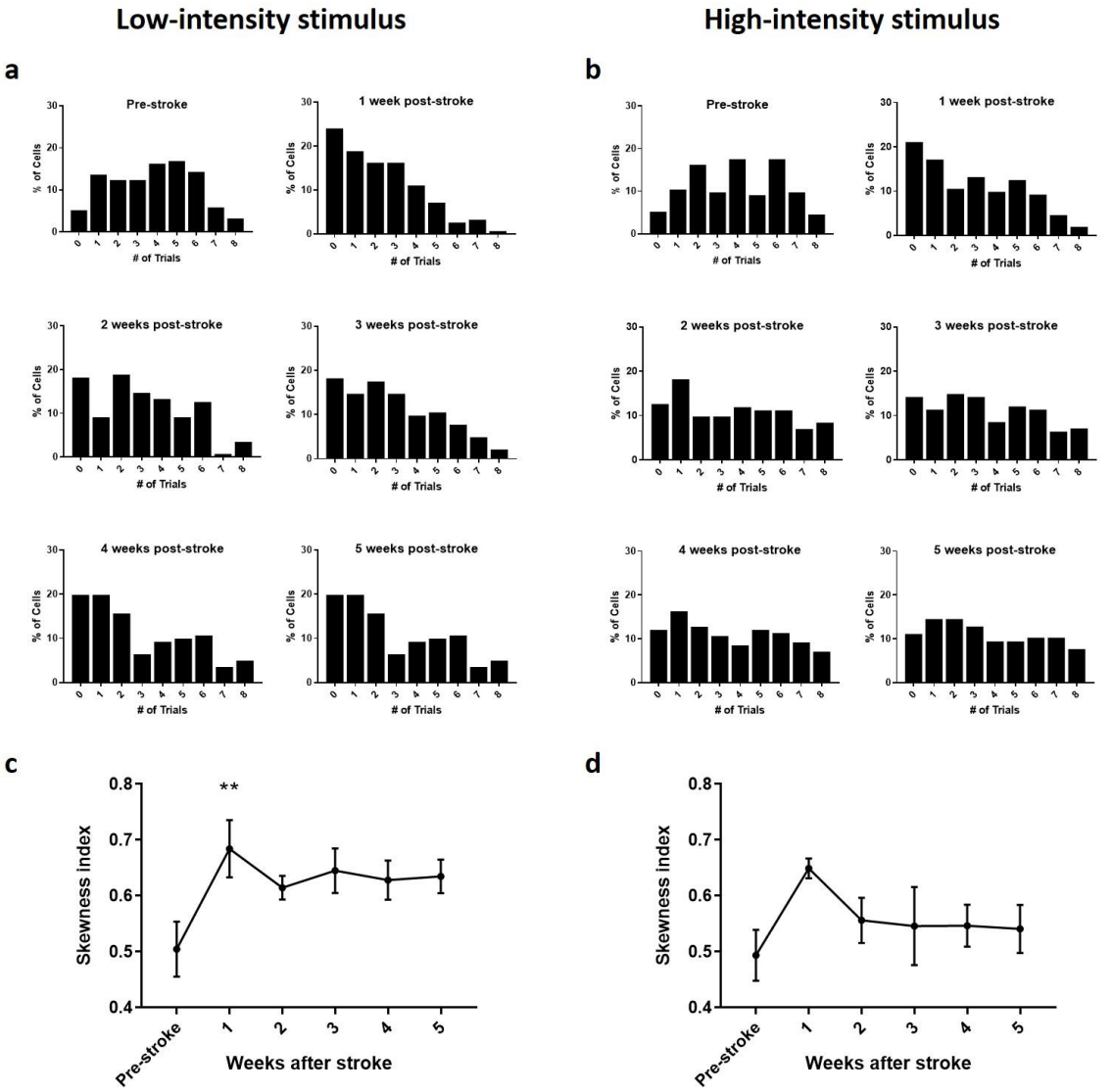

Figure 7. Frequency distribution of VIP-neurons response fidelity

(a-b) The fraction of sampled neurons (< 400 μm from infarct border) is plotted against their response fidelity (number of responsive trials out of 8 trials) at pre- and post-stroke imaging time-points for responses to low- and high-intensity stimulations, respectively.

(c-d) “Skewness Index” for graphs in (a) and (b) is calculated and plotted over time. Data are means ± S.E.M. * P<0.05; ** P<0.01; *** P<0.001 based on repeated measures one-way ANOVA and *post-hoc* t-tests comparing post-stroke time points relative to pre-stroke.

Our data has revealed at the population level, that there is an overall reduction in sensory-evoked responsiveness of peri-infarct neurons that is particularly robust one week after stroke. However, given that individual neurons inherently exhibit different levels of activity and response fidelity, we sought to determine if the overall reduction in responsiveness after stroke was the result of a uniform decrease in the whole population or comprised of different sub-populations of cells reacting variably to ischemic damage. Accordingly, we classified peri-infarct neurons into three distinct groups based on their pre-stroke levels of responsiveness and followed the fate of each group independently. Classification of cells was done based on the number of their responsive trials at pre-stroke such that cells with 0, 1, 2 responsive trials, cells with 3, 4, 5 responsive trials, and cells with 6, 7, 8 responsive trials were grouped as “Minimally responsive” (stroke, n=48; control, n=44), “Moderately responsive” (stroke, n=70; control, n=31) and “Highly responsive” (stroke, n=36; control, n=41), respectively. Interestingly 33% of highly responsive neurons, became minimally responsive after one week recovery from stroke (note black shaded bars in top row of Fig. 8a and 9a) which was not found in sham stroke controls. During the remaining recovery period, the fraction of these now minimally responsive neurons was progressively reduced, particularly by 5 weeks. Moderately responsive neurons appeared equally as likely to become highly or minimally responsive during the recovery period (middle row in Fig. 8a and 9a). While most minimally

responsive neurons remained in the same category over 5 weeks recovery, we were surprised to note that a fraction of these neurons became more responsive, some even highly responsive after stroke (bottom row of Figure 8a and 9a). A minimally responsive neuron that switches to a highly responsive one after stroke is exemplified in Figure 8b. In order to quantify these categorical changes over time, we calculated the mean number of responsive trials from 1 to 3 weeks post-stroke in each of the 3 categories of VIP neurons and then normalized that to the baseline/pre-stroke values both in sham control or stroke affected mice (Fig. 8c and 9b). Our analysis indicates that highly responsive neurons respond to significantly fewer stimulation trials after stroke (see left panel in Fig. 8c and 9b for both low and high intensity stimulation) whereas moderately responsive cells are less affected by stroke. Second, minimally responsive neurons are more likely to become responsive to stimulation trials after stroke, especially if the stimulation intensity is high (see right panels in Fig. 8c and 9b). These observations suggest that stroke differentially affects the response fidelity of these 3 categories of neurons. Furthermore, our data suggest the possibility that stroke can, in some cases, flip the polarity of VIP neuron responsiveness (On vs OFF) in sensory cortex.

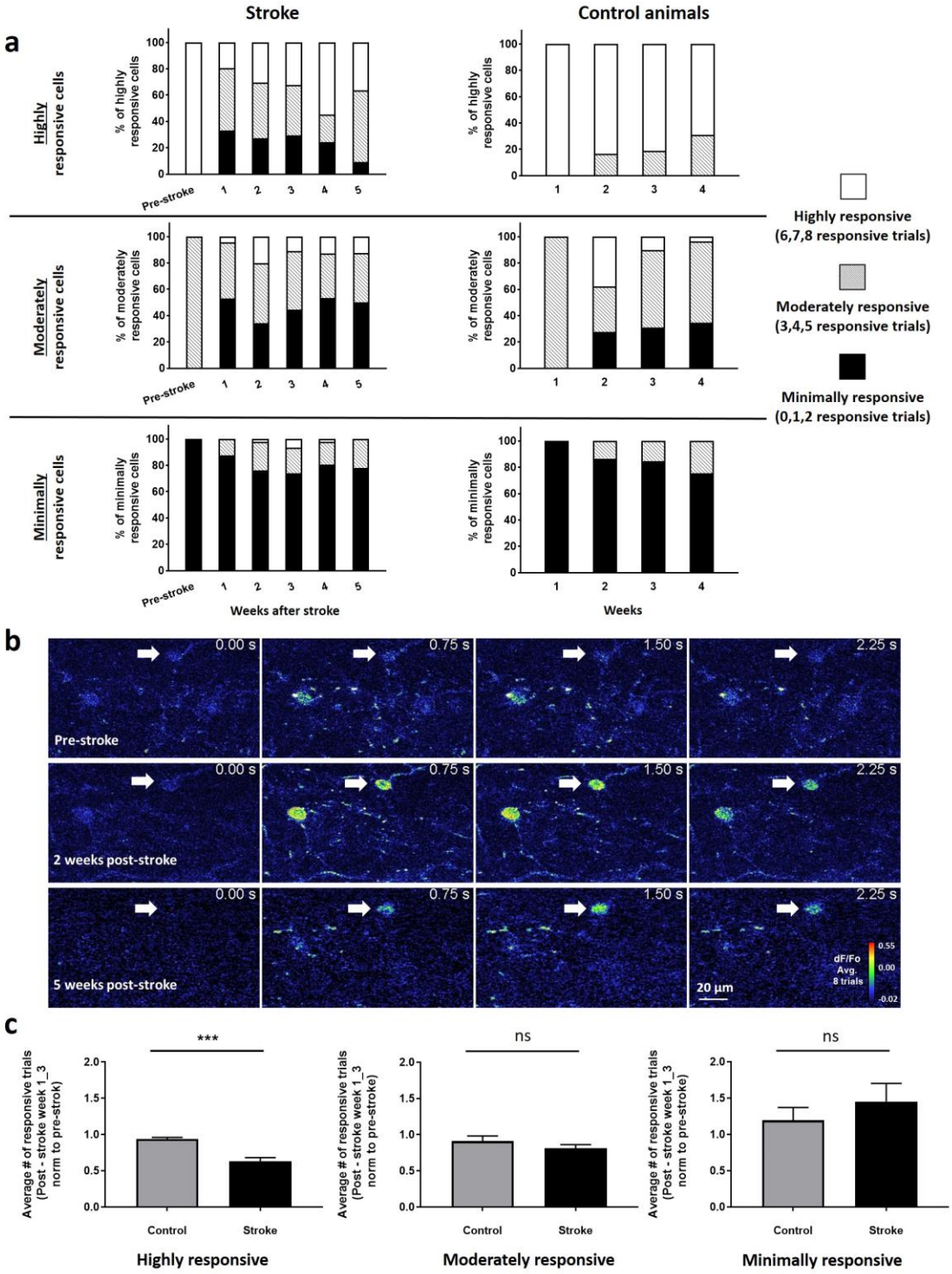
a
Stroke
Control animals
Highly responsive cells
Moderately responsive cells
Minimally responsive cells
% of highly responsive cells
% of moderately responsive cells
% of minimally responsive cells
Pre-stroke
Weeks after stroke
Weeks
Highly responsive (6,7,8 responsive trials)
Moderately responsive (3,4,5 responsive trials)
Minimally responsive (0,1,2 responsive trials)
b
0.00 s
0.75 s
1.50 s
2.25 s
Pre-stroke
2 weeks post-stroke
5 weeks post-stroke
dF/Fo Avg. 8 trials
20 µm
c
Average # of responsive trials (Post - stroke week 1_3 norm to pre-strok)
Average # of responsive trials (Post - stroke week 1_3 norm to pre-stroke)
***
ns
Control
Stroke
Highly responsive
Moderately responsive
Minimally responsive

Figure 8. Stroke unmasks sensory responsiveness in some neurons and silences others. Low intensity stimulation

(a) The population of sampled neurons (< 400 µm from infarct border) was classified into three groups based on their response fidelity at pre-stroke imaging session. Cells with 0, 1, 2 responsive trials, cells with 3, 4, 5 responsive trials, and cells with 6, 7, 8 responsive trials were grouped as "Minimally responsive" (stroke, n=48; control, n=44), "Moderately responsive" (stroke, n=70; control, n=31), and "Highly responsive" (stroke; n=36; control, n=41), respectively. Bar graphs display functional changes in each group for stroke (left) and sham stroke control (right) group. **(b)** Forelimb-evoked calcium responses of an example cell (averaged over 8 trials) that switches from minimally responsive to highly responsive. Scale bar, 20 µm. **(c)** Bar graphs indicate the average number of responsive trials (norm to pre-stroke) for each group of cells over three post-stroke weeks for stroke group and three weeks (week 2-4) for the sham stroke control group. Data are means ± S.E.M. * $P<0.05$; ** $P<0.01$; *** $P<0.001$ based on unpaired t-tests comparing stroke versus control group.

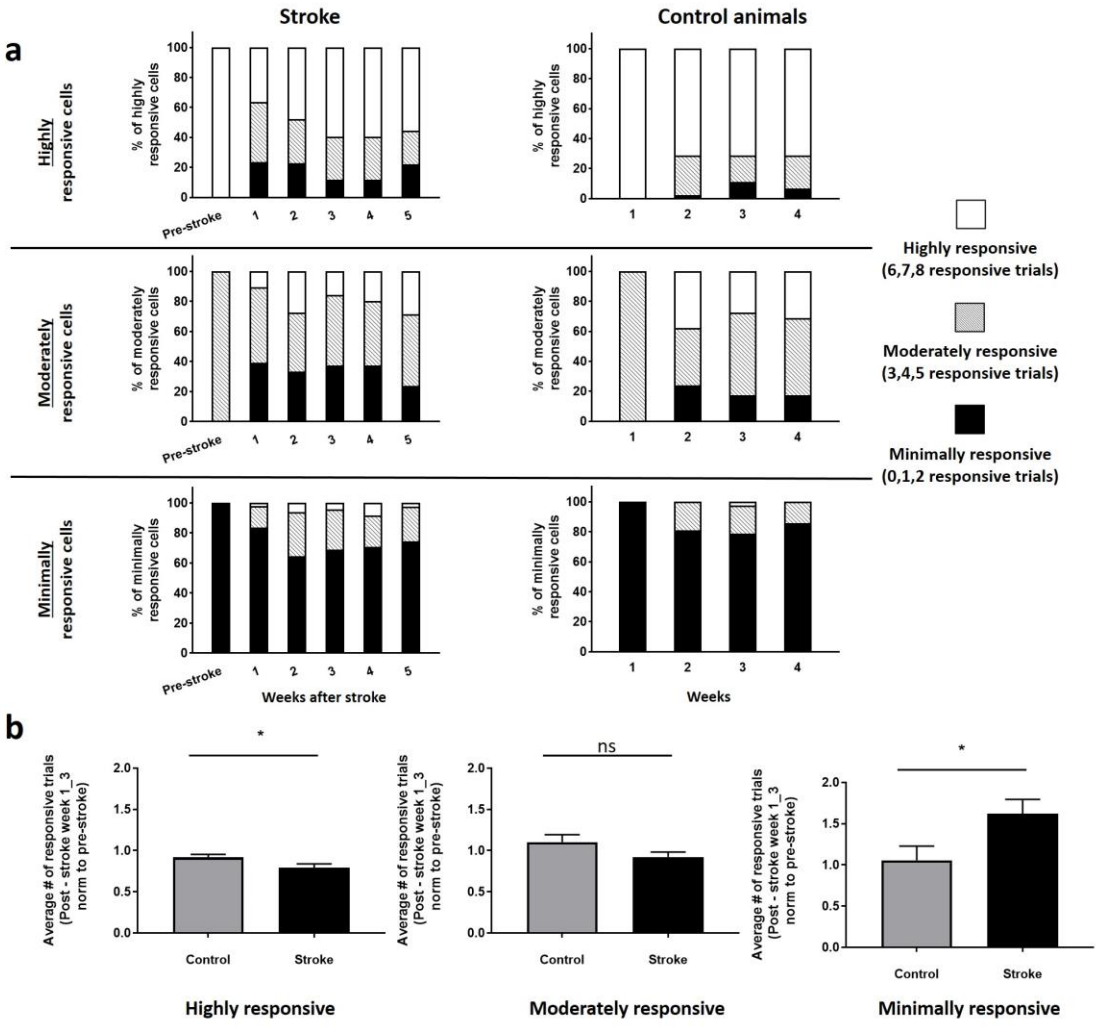

Figure 9. Stroke unmasks sensory responsiveness in some neurons and silences others. <u>High intensity stimulation</u>

(a) The population of sampled neurons (< 400 µm from infarct border) was classified into three groups based on their response fidelity at pre-stroke imaging session. Cells with 0, 1, 2 responsive trials, cells with 3, 4, 5 responsive trials, and cells with 6, 7, 8 responsive trials were grouped as "Minimally responsive" (stroke, n=48; control, n=44), "Moderately responsive" (stroke, n=70; control, n=31), and "Highly responsive" (stroke; n=36; control, n=41), respectively. Bar graphs display functional changes in each group for stroke (left) and sham stroke control (right) group. **(b)** Bar graphs indicate the average number of responsive trials (norm to pre-stroke) for each group of cells over three post-stroke weeks for stroke group and three weeks (week 2-4) for the sham stroke control group. Data are means ± S.E.M. * P<0.05; ** P<0.01; *** P<0.001 based on unpaired t-tests comparing stroke versus control group.

3.4 Stroke disrupts the predictability of sensory-evoked responses

Analysis of sensory-evoked responses in control animals suggested that VIP interneurons maintain a relatively reliable response fidelity (defined as a cell's number of responsive trials in an imaging session) over weeks. On the account of this observation, we sought to investigate whether this predictable neuronal response fidelity was preserved following ischemia. As illustrated in Figure 10a,b the pre-stroke fidelity of low and high intensity driven responses for individual neurons (peri-infarct area, <400μm) was determined (neurons were divided into nine groups representing zero to eight responsive trials at baseline/pre-stroke) and then followed for 4-5 weeks. The heat map in Figure 10a, visually illustrates the extent to which the response fidelity of each group of neurons deviates from their pre-stroke values over weeks. It also color codes the fraction of cells that underwent deviations in their response fidelity during each weekly imaging sessions. As one can note from this graph, the % of neurons that remain close to their baseline/pre-stroke response fidelity is higher in the sham stroke controls than the stroke group (note warmer colors at week 1 or 2 in controls versus stroke). By contrast, the spread of the population over time is much greater in the stroke group (note the wide spread of cool colors at each post-stroke week). This spread in response fidelity after stroke was reflected in a significant increase in the variance of responses pooled over 4 weeks (Fig. 10c,left and Fig.10d, left) or week to week variance (Fig. 10c,right and Fig. 10d,right). Collectively, these findings demonstrate a comparatively higher variance and decreased predictability of sensory-evoked neuronal responses after stroke, which may have important consequences for sensory perception and motor functions.

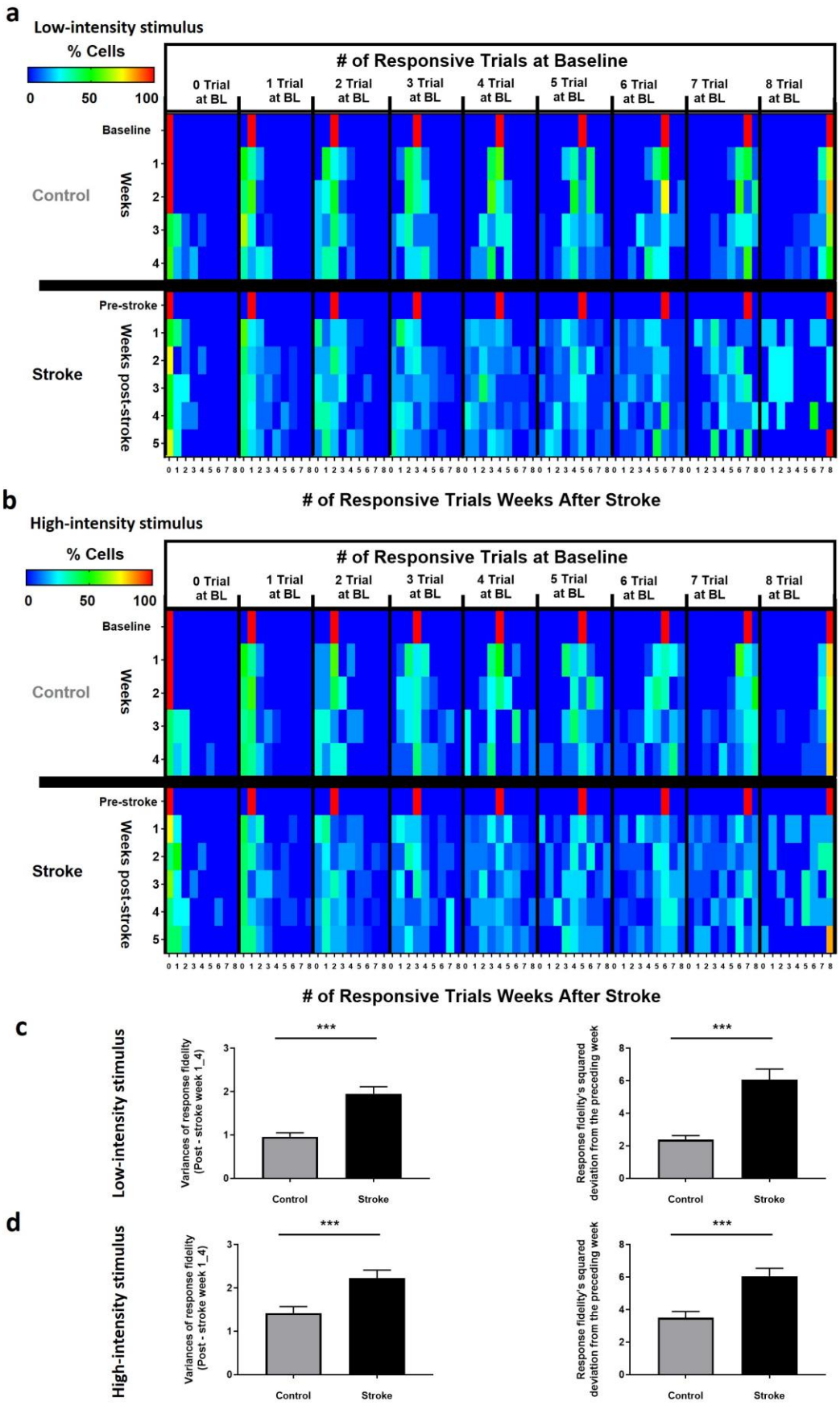
a
Low-intensity stimulus
% Cells
0
50
100
# of Responsive Trials at Baseline
0 Trial at BL
1 Trial at BL
2 Trial at BL
3 Trial at BL
4 Trial at BL
5 Trial at BL
6 Trial at BL
7 Trial at BL
8 Trial at BL
Baseline
Control
Weeks
Pre-stroke
Stroke
Weeks post-stroke
# of Responsive Trials Weeks After Stroke
b
High-intensity stimulus
% Cells
0
50
100
# of Responsive Trials at Baseline
0 Trial at BL
1 Trial at BL
2 Trial at BL
3 Trial at BL
4 Trial at BL
5 Trial at BL
6 Trial at BL
7 Trial at BL
8 Trial at BL
Baseline
Control
Weeks
Pre-stroke
Stroke
Weeks post-stroke
# of Responsive Trials Weeks After Stroke
c
Low-intensity stimulus
Variances of response fidelity (Post - stroke week 1_4)
***
Control
Stroke
Response fidelity's squared deviation from the preceding week
***
Control
Stroke
d
High-intensity stimulus
Variances of response fidelity (Post - stroke week 1_4)
***
Control
Stroke
Response fidelity's squared deviation from the preceding week
***
Control
Stroke

Figure 10. Stroke disrupts the predictability of sensory responses

(a,b) The population of sampled neurons (< 400 μm from infarct border) was classified into nine groups based on their baseline/pre-stroke response fidelity. Heat-maps displays changes in response fidelity of the exact same population of cells in each group over weeks. The fraction of cells that underwent deviations in their response fidelity is color coded; Colder and warmer colours represent lower and higher fractions of cells, respectively. Data in (a) and (b) correspond to analysis of responses to low and high intensity stimulation. **(c,d)** Left**,** average variances in response fidelity over four weeks after stroke (post-stroke week1-4, n = 154 cells) compared to similar values over four weeks in the sham stroke control group (n = 116). Right, the average of squared differences in response fidelity between subsequent weeks was calculated. Bar graphs comparing these values over five weeks after stroke (post-stroke week1-5, n = 154) and four weeks in sham stroke control group (n = 116). Data in (c) and (d) correspond to analysis of responses to low and high intensity stimulation. Data are means ± S.E.M. * $P<0.05$; ** $P<0.01$; *** $P<0.001$ based on an unpaired t-test comparing stroke versus control group.

3.5 Stroke leads to lower levels of spontaneous activity in VIP neurons

To supplement our analysis of sensory-evoked VIP neuron activity, we examined the spontaneous activity of neurons (same cells as in the analysis of sensory-evoked responses) before and until five weeks after stroke. Calcium transients were recorded over a 75 s period with no stimulation in each imaging area (Fig. 11a). Similar to the analysis of sensory-evoked responses, spontaneous calcium traces were extracted from each cell body and corrected for potential neuropil contamination. ΔF/Fo was calculated for each calcium trace where Fo was set to be the 30th percentile value of each individual trace. Subsequently, parts of each trace that were associated with a calcium event was identified (*see methods*). We used the total number of events "Number of events" and the total time associated with all events "Active time" in each trace as two measures of spontaneous activity (Figure 11b). As is shown in Figure 11c, there was a reduction in the spontaneous activity of VIP neurons one week after the stroke. However levels of spontaneous activity thereafter appeared to recover and were statistically indistinguishable from pre-stroke levels. These results show that stroke has a very transient effect on spontaneous activity levels.

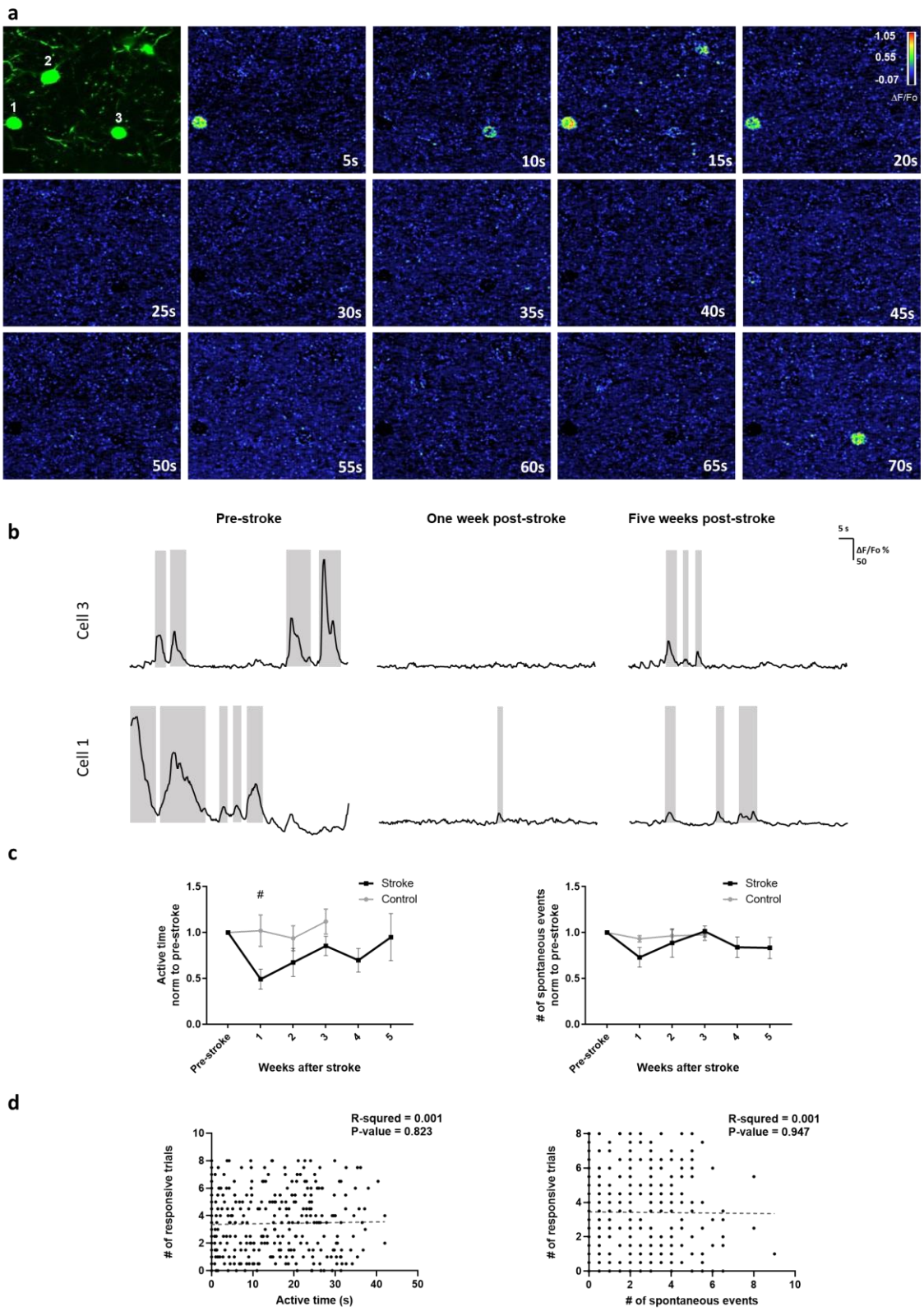
a
1
2
3
1.05
0.55
-0.07
ΔF/Fo
5s
10s
15s
20s
25s
30s
35s
40s
45s
50s
55s
60s
65s
70s
b
Pre-stroke
One week post-stroke
Five weeks post-stroke
5 s
ΔF/Fo %
50
Cell 3
Cell 1
c
Stroke
Control
#
Active time norm to pre-stroke
# of spontaneous events norm to pre-stroke
Pre-stroke
Weeks after stroke
d
R-squred = 0.001
P-value = 0.823
# of responsive trials
Active time (s)
R-squred = 0.001
P-value = 0.947
# of spontaneous events

Figure 11. Stroke leads to lower levels of spontaneous activity

(a) Colour montages show spontaneous changes in GCaMP6s fluorescence (ΔF/Fo) of neurons in an example area over 70 s imaging period. Changes in GCaMP6s fluorescence is shown in 5 s intervals. Note that, some cells exhibit more spontaneous activity, indicated by arrowheads. Scale bar, 20 µm. **(b)** Calcium traces extracted from cell 1 and cell 3 in (a) before and at different time-points after stroke. Gray areas on each trace show the period of time when signal is identified as active (calcium event). **(c) "**Active time" (left) and "Number of events" (right) for the population of sampled neurons (< 400 µm from infarct border) are plotted against time after stroke (n = 6 stroke mice; n = 4 control mice). **(d)** Graphs show the relationship between spontaneous activity (Active time, left; number of spontaneous events, right) and sensory evoked activity (number of responsive trials) at pre-stroke imaging session. There was no correlation between sensory responsiveness and the level of spontaneous activity. Data are means ± S.E.M. * P<0.05; ** P<0.01; *** P<0.001 based on two-way ANOVA comparing stroke versus control at each time-point. # P<0.05; ## P<0.01; ### P<0.001 based on one-way ANOVA comparing post-stroke time-points in each graph relative to pre-stroke values.

4 _ Discussion

4.1 Overview

Previous examination of sensory-evoked cortical hemodynamic responses and aggregate neuronal activity (using VSD) demonstrated that sensory-evoked cortical responses in the stroke-affected hemisphere are significantly diminished in the first 1-2 weeks after the insult. Moreover, the lack of cortical responsiveness to tactile sensory stimulation coincides with maximal sensorimotor deficits (Dijkhuizen et al., 2001; Brown et al., 2009; Winship and Murphy, 2009). Consistent with this evidence, our imaging experiments revealed that one week after the stroke, there was a significant reduction in the percentage of VIP neurons that were responsive to FL touch (Fig. 4d,e and 5a,b). The reduction depended, in part, on the strength of the stimulation intensity since there was a ~60% reduction in the low-intensity stimulation group verses ~30% in the high-intensity group. The percentage of FL responsive trials (~38% in the low-intensity group; ~25% in the high-intensity group), and average response amplitude were also reduced in the first week after stroke (Fig 5a,b).

Diminished cortical responsiveness can be attributed to both functional and structural alterations in the post-ischemic brain. Following ischemic damage, neurons in the surviving peri-infarct tissue lose many of their local connections from neurons within the necrotic core. In addition, since the stroke usually extends down to the corpus callosum, axons from the thalamus or other distant cortical regions that traverse through the corpus callosum (en route the somatosensory cortex), can be disrupted. Carmichael and colleagues showed that a small cortical stroke in the barrel cortex of rats can result in hypometabolism, reflecting a reduction in neuronal activity, in cortical regions both

distant (i.e. several millimeters from the infarct) and adjacent to necrotic ischemic core (Carmichael et al., 2004). They attributed this far reaching cortical hypometabolism to the disruption of neural connections. Therefore, partial loss of neural activity from the cortical infarct region could decrease cortical responsiveness in peri-infarct regions at one week after the stroke. Additionally, structural analysis of neuronal processes in perilesional cortical tissue has demonstrated that stroke gives rise to significant reductions in the number of synaptic structures, such as dendritic spines, axon terminals and synaptic vesicles, during the first 1-2 weeks following the insult (Corbett et al., 2006; Ito et al., 2006; Brown et al., 2007, 2009; Mostany et al., 2010). Accordingly, decreased sensory responsiveness that we observed during the first week after stroke could be explained by reductions in the number of functional synapses, diminished afferent drive from the infarct region or other stroke-related functional changes like excessive tonic GABAergic inhibition (Clarkson et al., 2010).

The return of cortical responses to sensory stimulation after stroke requires the establishment of new synaptic connections that enable routing of sensory signals to the surviving cortical regions. In agreement with this notion, ongoing recovery from stroke has been shown to be accompanied by heightened rates of synaptic turnover, as revealed by *in-vivo* imaging of dendritic spines (Ito et al., 2006; Brown et al., 2007; Mostany et al., 2010; Clark et al., 2019). Similar to the mechanisms involved in cortical plasticity in the developing or adult healthy brain, sensory experience plays a critical role in shaping newly formed compensatory circuits after stroke. Experience-dependent synaptic plasticity after stroke may involve long-term potentiation like changes in the synaptic strength of existing synapses, pruning of old synapses and stabilization of new synapses.

Similarities in the time course of post-stroke changes in synaptic structures and changes in neuronal responsiveness suggest that these phenomena may be directly related to each other (Brown et al., 2007; Mostany et al., 2010; Clark et al., 2019). Additionally, our data revealed that the reduction in the responsiveness of VIP neurons during the first week following stroke was primarily restricted to areas located within close proximity (<400 µm) to the infarct border (Fig. 6b,c). Consistent with our findings, changes in synaptic turnover rates have been reported to be mostly limited to areas within 500µm from the infarct core in a photothrombotic model of stroke in mice (Brown et al., 2007). Although the extent of functional and structural changes reported in different studies is largely dependent on the size, location and the model of stroke, most studies have reported the largest effect of stroke on synaptic functions and structures to be limited to areas within a couple of hundred micrometers from the ischemic border (Stroemer et al., 1995; Xerri et al., 1998; Cramer and Chopp, 2000; Biernaskie and Corbett, 2001; Carmichael et al., 2001; Carmichael, 2003; Gonzalez and Kolb, 2003; Brown et al., 2007).

To the best of our knowledge, our study is the first to longitudinally image and characterize sensory-driven responses in an inhibitory neural population over several weeks. Our imaging revealed that the fidelity of sensory-evoked responses in VIP neurons were heterogeneous and could change over time. Accordingly, we classified VIP neurons into three functional groups (highly, moderately and minimally responsive) and followed the fate of each group independently. In sham stroke control mice, we found that the response fidelity in these populations was relatively stable over five weeks of imaging. Stability in the fidelity of sensory-driven responses (over the span of 1 week) in

healthy mice has also been reported in excitatory somatosensory cortical neurons (Margolis et al., 2012). However, until conducting this study, it was unknown if stroke could lead to significant changes in the response fidelity of VIP neurons, let alone any neural population. In the present study, it was found that a large portion of highly responsive neurons (33%), became minimally responsive after one week recovery from stroke (Fig. 8a and 9a). During the remaining recovery period, many of these neurons remained minimally responsive although it should be noted that small fraction shifted back into the moderately or highly responsive fraction by 5 weeks recovery. Moderately responsive neurons were equally likely to become highly or minimally responsive during the recovery period (Fig. 8a and 9a). While most minimally responsive neurons remained in the same category over 5 weeks of recovery, surprisingly a small fraction of these neurons became responsive to FL stimulation (Figure 8a and 9a). These observations suggest that stroke can, in some cases, flip the polarity of VIP neuron responsiveness (On vs Off) in sensory cortex, by recruiting minimally active neurons, either through the sprouting of new synaptic connections or by unmasking previously silent VIP circuits. Recruitment of inactive, 'silent' neurons has previously been proposed as a mechanism involved in shifting cortical receptive field maps after sensory deprivation or injury (Brecht et al., 2005; Shoham et al., 2006; Margolis et al., 2012).

The reported changes in the response fidelity of VIP neurons in my study parallels those from a recent *in-vivo* longitudinal calcium imaging study in layer 2/3 barrel cortex neurons. The Helmchen group showed that trimming of all but one whisker resulted in differential changes in neuronal responsiveness across functionally distinct subpopulations of putative excitatory neurons. Specifically, they reported that neurons

classified as “highly responsive” to whisker stimulation, were most likely to be disrupted by whisker trimming and show the largest decrease in response amplitude. Conversely, neurons classified as “low” responders to whisker stimulation were most likely to become “responsive” neurons in the spared/un-deprived cortical region. Based on these observations they came up with a ‘reduce and distribute’ model of plasticity where a convergent redistribution of activity engaged a larger fraction of neurons in the sensory task without a dramatic change in overall population activity (Margolis et al., 2012). Although drawing an analogy between plasticity mechanisms in a healthy and stroke-affected brain is tenuous, it is conceivable that stroke induced changes in sensory maps in peri-infarct tissue may follow the same basic model of activity redistribution (toward the middle from both high and low responsive cells).

While no previous study has repeatedly imaged the same population of neurons before and after a stroke, an *in-vivo* calcium imaging study from the Murphy lab examined sensory-evoked responses in cortical neurons at single time-points after focal stroke in forelimb somatosensory cortex. Similar to our study, they showed that 2 weeks after stroke, neurons in the surviving portion of the FL cortex became unresponsive to FL stimulation. However at 1 and 2 months recovery, peri-infarct neurons became responsive to stimulation of multiple limbs and therefore were less selective for a preferred limb (Winship et al., 2008). This reduction in neuronal selectivity was most evident in the border regions between FLS1 and HLS1 and was thought to be a transitory period preceding the development of new functional roles (Winship et al., 2008). While our study did not characterize response selectivity to different limbs, it is possible that the observed reduction in VIP neuron response fidelity to FL stimulation could be related to

the possibility that these neurons are now responsive to other sensory inputs. One mechanism suggested to explain decreased peri-infarct response selectivity during this period is that stroke-induced disruptions in inhibitory circuits may unmask the synaptic inputs from other limbs. In this scenario, sensory inputs that previously elicited only subthreshold changes in membrane potential now lead to suprathreshold firing after stroke.

An interesting and potentially significant finding in our study was that stroke led to more variable and therefore less predictable sensory-evoked neuronal responses in VIP neurons (Fig. 10 a,b). It should be noted that comparable levels of spontaneous activity across weeks in stroke vs control mice rule out the possibility that increased variances in response fidelity are simply a consequence of increased spontaneous activity. Decreased response predictability may have important consequences for the perception of sensory inputs and motor functions after stroke. Analysis of neuronal responses in later time-points (> 5 weeks) is required to test whether robust response fidelity is eventually restored after stroke. If response fidelity is never restored, it could conceivably limit any further recovery in somatosensory function. Future studies that seek to improve stroke recovery should consider variances in sensory response fidelity, or at the very least measure and report it if possible. From a mechanistic viewpoint, the causes of VIP neuron response uncertainty are speculative in nature. For example, the destabilization of synaptic structures and proliferation of synapses on VIP neurons in the first few weeks after stroke (unpublished observations from Brown lab) may also be a reason for the emergence of aberrant and non-predictable sensory responses in peri-infarct VIP neurons (Brown et al., 2007; Mostany et al., 2010; Fu et al., 2012; Clark et al., 2019).

Alternatively, it could be suggested that heightened variances of VIP responses after stroke are a consequence of extrinsic factors, such as neuromodulatory circuits (cholinergic, noradrenergic, dopaminergic neurotransmission, etc) that influence the activity and synchrony of sensory cortical neurons. Future studies will be needed to address these specific hypotheses.

4.2 Diminished VIP release

In addition to GABA mediated dis-inhibitory functions of VIP neurons, these neurons have been shown to be involved in an array of cortical functions by releasing neuromodulators such as VIP (White et al., 2010). VIP is a peptide hormone that demonstrates important vasodilatory roles in the brain. Previous studies have shown that VIP neurons can transmute neuronal signals into vascular response by secreting VIP (Cauli et al., 2004). Reductions in the activity levels of VIP neurons after stroke may shift the probability of VIP release that requires high frequency neuronal activity. Decreased VIP release, in turn, may lead to long-term reductions in peri-infarct blood perfusion which has been reported to be crucial for synaptic plasticity and functional recovery after stroke (Mostany et al., 2010). Accordingly, it is yet to be investigated to what extent the disruption in VIP neurons activity observed in this study may influence VIP vs GABA transmission.

4.3 Limitations

4.3.1 Inferring neuronal activity from calcium-dependent changes in GCaMP6s fluorescence

Calcium imaging is a powerful approach for non-invasive recording of the *in-vivo* activity of identified cells (including cortical neurons) over chronic timescales (Chen et al., 2013). One limitation associated with this technique is that cellular activity is inferred

indirectly from changes in free intracellular calcium levels. Therefore, alterations in the dynamics of calcium transients may distort measurements of neuronal activity. More importantly, the non-linear relationship between spiking activity and changes in the fluorescence of calcium indicator, complicates the interpretation of imaging results. Binarizing calcium signals into ‘responsive’ or ‘not responsive’ as we did for each trial and cell, can minimize the effects of nonlinearity associated with calcium imaging. In this approach, activity levels are examined by the presence of events in response to sensory stimulation rather than their size. In the present study, we made use of the calcium indicator GCaMP6s in order to assess VIP neurons activity. Although GCaMP6s demonstrates high detection rates for single action potentials (~ 99% at 1% false positive rate), it has relatively slow kinetics compared to other GECIs such as GCaMP6f (Chen et al., 2013). Due to the slow kinetics of GCaMP6s, resolving individual spikes is impossible if the time interval between spikes are short (<150 ms). In this case, the spiking activity is only inferred from the amplitude of fluorescent response which is non linearly correlated to firing rate.

4.3.2 Anesthesia

We collected our imaging data under light anesthesia using isoflurane. Depending on the type and the concentration of the drug, anesthesia may disrupt aspects of neuronal communications (Richards, 1983; Seto et al., 2014). Isoflurane in particular, has previously been shown to be capable of modulating excitatory and inhibitory synaptic transmission and thereby altering both baseline and stimulus-evoked neuronal activity (De Sousa et al., 2000; Aksenov et al., 2015). Especially, the activity levels of VIP neurons is shown to be modulated by attention and arousal during periods of behavioural

engagement (Pi et al., 2013; Fu et al., 2014; Kuchibhotla et al., 2017). Accordingly, it could be conceivable that sensory response properties of VIP neurons may be different between periods of anesthesia and wakefulness.

4.3.3 Passive stimulation

In this study, we examined sensory-evoked transients in response to a passive FL stimulation (vibrating stimulus). However, the perception of tactile sensory experience involves an active sensory component related to self-movement of the limb on an object (Gibson, 1962). Accordingly, stroke-related changes in response properties of neurons to the passive stimulation of FL may not demonstrate the influence of stroke on tactile sensation. Additionally, since animals in our study were not tested behaviourally, the relationship between alterations in sensory-driven response properties and sensorimotor functions is yet to be revealed.

4.3.4 Layer-dependent differences

Imaging of VIP neuron activity in our study was mostly restricted to superficial layers. Although the majority of VIP neurons (~60%) are distributed in layer (II/III), previous studies have shown that VIP neurons exhibit layer-dependent differences in their morphological and electrophysiological properties. Layer II/III VIP neurons project their dendritic branches to Layers I and II/III and their axons span all cortical layers, whereas layer IV-VI VIP neurons extend their dendritic branches throughout all cortical layers with their axons mostly restricted to layer V and VI (Prönneke et al., 2015). Additionally, VIP neurons show layer-dependent variability in their firing patterns and resting membrane potentials (Prönneke et al., 2015). Given these differences, our

imaging data from superficial layers may not be representative of stroke-related changes in the whole population of VIP neurons across different cortical layers.

4.4 Future directions

There has been accumulating evidence that increased levels of GABAergic synaptic transmission in the peri-infarct region impedes mechanisms involved in experience-dependent rewiring of peri-infarct cortical tissue and limits recovery of limb function. Therefore, decreasing inhibitory transmission (upregulating cortical excitability) after stroke may facilitate network plasticity and improve the recovery of lost sensorimotor functions. In keeping with this idea, clinical studies demonstrated that upregulating cortical excitability by direct or external stimulation of the perilesional brain tissue using rTMS or tDCS enhanced the beneficial effects of rehabilitative training on brain plasticity (Nitsche et al., 2003; Butefisch et al., 2004; Hummel et al., 2005; Kim et al., 2006; Fritsch et al., 2010). Additionally, it has been shown that suppressing GABAergic transmission by pharmacological blockage of GABA receptors significantly enhances sensorimotor performance after stroke both in human and animal models (Clarkson et al., 2010; Lake et al., 2015; Alia et al., 2016). Although pharmacological downregulation of GABAergic signalling is a promising intervention, due to the ubiquitous influence of GABA in brain functions and the lack of spatial control over drug delivery, these strategies are often either accompanied by undesired side effects (e.g. epilepsy), or by only partial improvements in behavioural performance. Therefore,

developing new methods for controlling inhibition in a more systematically restricted manner is required.

Based on the existing literature, it is conceivable that stroke-related changes in cortical excitability may be governed by concomitant changes in the activity of inhibitory circuits. Examining stroke-related changes in distinct classes of inhibitory neurons is, therefore, critical for achieving a better understanding of the mechanisms involved in post-stroke alterations in cortical excitability. In particular, due to their important roles in regulating cortical excitability, sensory modulation, and adult plasticity, examination of dis-inhibitory components could be of paramount importance. It has been shown that activity levels in VIP neurons are correlated with the activity level of local excitatory networks. Accordingly, it is conceivable that decreased activity in VIP neurons (observed in our study) over weeks after stroke may further contribute to the suppression of cortical network excitability in the peri-infarct regions. Based on these observations, one could hypothesize that enhancing the activity of VIP neurons may promote the recovery of functions after stroke by reducing excessive GABAergic transmission by other inhibitory neurons, and thereby upregulating the excitability of cortical networks. Fortunately, advances in chemogenetic and optogenetic techniques has enabled testing of these ideas by allowing targeted modulation of neural activity levels *in-vivo*, in defined neuronal subtypes (including VIP neurons) within defined regions of the brain. Considering the restricted effect of dis-inhibitory circuits on local excitatory networks, targeted modulation of VIP neurons in the peri-infarct regions (where rewiring happens), will likely be a better method for manipulating post-stroke inhibition without systematic side-effects of other methods.

Bibliography

Aksenov, D. P., Li, L., Miller, M. J., Iordanescu, G., & Wyrwicz, A. M. (2015). Effects of anesthesia on BOLD signal and neuronal activity in the somatosensory cortex. *Journal of Cerebral Blood Flow and Metabolism*. https://doi.org/10.1038/jcbfm.2015.130

Alia, C., Spalletti, C., Lai, S., Panarese, A., Micera, S., & Caleo, M. (2016). Reducing GABA A-mediated inhibition improves forelimb motor function after focal cortical stroke in mice. *Scientific Reports*. https://doi.org/10.1038/srep37823

Baroncelli, L., Sale, A., Viegi, A., Maya Vetencourt, J. F., De Pasquale, R., Baldini, S., & Maffei, L. (2010). Experience-dependent reactivation of ocular dominance plasticity in the adult visual cortex. *Experimental Neurology*. https://doi.org/10.1016/j.expneurol.2010.08.009

Bear, M. F., & Singer, W. (1986). Modulation of visual cortical plasticity by acetylcholine and noradrenaline. *Nature*. https://doi.org/10.1038/320172a0

Biernaskie, J., & Corbett, D. (2001). Enriched rehabilitative training promotes improved forelimb motor function and enhanced dendritic growth after focal ischemic injury. *Journal of Neuroscience*. https://doi.org/10.1523/jneurosci.21-14-05272.2001

Brecht, M., Schneider, M., & Manns, I. D. (2005). Silent neurons in sensorimotor cortices: Implications for cortical plasticity. In *Neural Plasticity in Adult Somatic Sensory-Motor Systems*.

Brown, C. E., Aminoltejari, K., Erb, H., Winship, I. R., & Murphy, T. H. (2009). In vivo voltage-sensitive dye imaging in adult mice reveals that somatosensory maps lost to stroke are replaced over weeks by new structural and functional circuits with prolonged modes of activation within both the peri-infarct zone and distant sites. *Journal of Neuroscience*. https://doi.org/10.1523/JNEUROSCI.4249-08.2009

Brown, C. E., Boyd, J. D., & Murphy, T. H. (2010). Longitudinal in vivo imaging reveals balanced and branch-specific remodeling of mature cortical pyramidal dendritic arbors after stroke. *Journal of Cerebral Blood Flow and Metabolism*. https://doi.org/10.1038/jcbfm.2009.241

Brown, C. E., Li, P., Boyd, J. D., Delaney, K. R., & Murphy, T. H. (2007). Extensive turnover of dendritic spines and vascular remodeling in cortical tissues recovering from stroke. *Journal of Neuroscience*. https://doi.org/10.1523/JNEUROSCI.4295-06.2007

Brown, C. E., Wong, C., & Murphy, T. H. (2008). Rapid morphologic plasticity of peri-infarct dendritic spines after focal ischemic stroke. *Stroke*. https://doi.org/10.1161/STROKEAHA.107.498238

Bütefisch, C. M., Khurana, V., Kopylev, L., & Cohen, L. G. (2004). Enhancing Encoding of a Motor Memory in the Primary Motor Cortex by Cortical Stimulation. *Journal of Neurophysiology*. https://doi.org/10.1152/jn.01038.2003

Carmichael, S. T. (2005). Rodent models of focal stroke: Size, mechanism, and purpose. *NeuroRx*. https://doi.org/10.1602/neurorx.2.3.396

Carmichael, S. T. (2006). Cellular and molecular mechanisms of neural repair after stroke: Making waves. *Annals of Neurology*. https://doi.org/10.1002/ana.20845

Carmichael, S. T. (2003). Plasticity of cortical projections after stroke. *Neuroscientist*. https://doi.org/10.1177/1073858402239592

Carmichael, S. T., Tatsukawa, K., Katsman, D., Tsuyuguchi, N., & Kornblum, H. I. (2004). Evolution of Diaschisis in a Focal Stroke Model. *Stroke*. https://doi.org/10.1161/01.STR.0000117235.11156.55

Castro-Alamancos, M. A., & Borrell, J. (1995). Functional recovery of forelimb response capacity after forelimb primary motor cortex damage in the rat is due to the reorganization of adjacent areas of cortex. *Neuroscience*. https://doi.org/10.1016/0306-4522(95)00178-L

Cauli, B., Tong, X. K., Rancillac, A., Serluca, N., Lambolez, B., Rossier, J., & Hamel, E. (2004). Cortical GABA interneurons in neurovascular coupling: Relays for subcortical vasoactive pathways. *Journal of Neuroscience*. https://doi.org/10.1523/JNEUROSCI.3065-04.2004

Chen, S. X., Kim, A. N., Peters, A. J., & Komiyama, T. (2015). Subtype-specific plasticity of inhibitory circuits in motor cortex during motor learning. *Nature Neuroscience*. https://doi.org/10.1038/nn.4049

Chen, T. W., Wardill, T. J., Sun, Y., Pulver, S. R., Renninger, S. L., Baohan, A., … Kim, D. S. (2013). Ultrasensitive fluorescent proteins for imaging neuronal activity. *Nature*. https://doi.org/10.1038/nature12354

Clark, T. A., Sullender, C., Jacob, D., Zuo, Y., Dunn, A. K., & Jones, T. A. (2019). Rehabilitative training interacts with ischemia-instigated spine dynamics to promote a lasting population of new synapses in peri-infarct motor cortex. *The Journal of Neuroscience*. https://doi.org/10.1523/jneurosci.1141-19.2019

Clarkson, A. N., Huang, B. S., MacIsaac, S. E., Mody, I., & Carmichael, S. T. (2010). Reducing excessive GABA-mediated tonic inhibition promotes functional recovery after stroke. *Nature*. https://doi.org/10.1038/nature09511

Corbett, D., Giles, T., Evans, S., McLean, J., & Biernaskie, J. (2006). Dynamic changes in CA1 dendritic spines associated with ischemic tolerance. *Experimental Neurology*. https://doi.org/10.1016/j.expneurol.2006.05.020

Crestani, F., Martin, J. R., Möhler, H., & Rudolph, U. (2000). Mechanism of action of the hypnotic zolpidem in vivo. *British Journal of Pharmacology*. https://doi.org/10.1038/sj.bjp.0703717

Dana, H., Chen, T. W., Hu, A., Shields, B. C., Guo, C., Looger, L. L., … Svoboda, K. (2014). Thy1-GCaMP6 transgenic mice for neuronal population imaging in vivo. *PLoS ONE*. https://doi.org/10.1371/journal.pone.0108697

Dancause, N., Barbay, S., Frost, S. B., Plautz, E. J., Chen, D., Zoubina, E. V., … Nudo, R. J. (2005). Extensive cortical rewiring after brain injury. *Journal of Neuroscience*. https://doi.org/10.1523/JNEUROSCI.3256-05.2005

De Sousa, S. L. M., Dickinson, R., Lieb, W. R., & Franks, N. P. (2000). Contrasting synaptic actions of the inhalational general anesthetics isoflurane and xenon. *Anesthesiology*. https://doi.org/10.1097/00000542-200004000-00024

Dijkhuizen, R. M., Ren, J., Mandeville, J. B., Wu, O., Ozdag, F. M., Moskowitz, M. A., … Finklestein, S. P. (2001). Functional magnetic resonance imaging of reorganization in rat brain after stroke. *Proceedings of the National Academy of Sciences of the United States of America*. https://doi.org/10.1073/pnas.231235598

Donato, F., Rompani, S. B., & Caroni, P. (2013). Parvalbumin-expressing basket-cell network plasticity induced by experience regulates adult learning. *Nature*. https://doi.org/10.1038/nature12866

Fagiolini, M., & Hensch, T. K. (2000). Inhibitory threshold for critical-period activation in primary visual cortex. *Nature*. https://doi.org/10.1038/35004582

Feigin, V. L., Forouzanfar, M. H., Krishnamurthi, R., Mensah, G. A., Connor, M., Bennett, D. A., … Naghavi, M. (2014). Global and regional burden of stroke during 1990-2010: Findings from the Global Burden of Disease Study 2010. *The Lancet*. https://doi.org/10.1016/S0140-6736(13)61953-4

Figueroa Velez, D. X., Ellefsen, K. L., Hathaway, E. R., Carathedathu, M. C., & Gandhi, S. P. (2017). Contribution of innate cortical mechanisms to the maturation of orientation selectivity in parvalbumin interneurons. *Journal of Neuroscience*. https://doi.org/10.1523/JNEUROSCI.2386-16.2016

Fritsch, B., Reis, J., Martinowich, K., Schambra, H. M., Ji, Y., Cohen, L. G., & Lu, B. (2010). Direct current stimulation promotes BDNF-dependent synaptic plasticity: Potential implications for motor learning. *Neuron*. https://doi.org/10.1016/j.neuron.2010.03.035

Frostig, R. D., Lieke, E. E., Ts'o, D. Y., & Grinvald, A. (1990). Cortical functional architecture and local coupling between neuronal activity and the microcirculation revealed by in vivo high-resolution optical imaging of intrinsic signals. *Proceedings of the National Academy of Sciences of the United States of America*. https://doi.org/10.1073/pnas.87.16.6082

Fu, Y., Kaneko, M., Tang, Y., Alvarez-Buylla, A., & Stryker, M. P. (2015). A cortical disinhibitory circuit for enhancing adult plasticity. *ELife*. https://doi.org/10.7554/eLife.05558

Fu, Y., Tucciarone, J. M., Espinosa, J. S., Sheng, N., Darcy, D. P., Nicoll, R. A., … Stryker, M. P. (2014). A cortical circuit for gain control by behavioral state. *Cell*. https://doi.org/10.1016/j.cell.2014.01.050

Fuxe, K., Bjelke, B., Andbjer, B., Grahn, H., Rimondini, R., & Agnati, L. F. (1997). Endothelin-1 induced lesions of the frontoparietal cortex of the rat. A possible model of focal cortical ischemia. *NeuroReport*. https://doi.org/10.1097/00001756-199707280-00040

Gentet, L. J., Kremer, Y., Taniguchi, H., Huang, Z. J., Staiger, J. F., & Petersen, C. C. H. (2012). Unique functional properties of somatostatin-expressing GABAergic neurons in mouse barrel cortex. *Nature Neuroscience*. https://doi.org/10.1038/nn.3051

Gerrow, K., & Brown, C. E. (2017). Structural Neural Plasticity During Stroke Recovery. In *The Rewiring Brain: A Computational Approach to Structural Plasticity in the Adult Brain*. https://doi.org/10.1016/B978-0-12-803784-3.00003-2

Gibson, J. J. (1962). Observations on active touch. *Psychological Review*. https://doi.org/10.1037/h0046962

Gonzalez, C. L. R., & Kolb, B. (2003). A comparison of different models of stroke on behaviour and brain morphology. *European Journal of Neuroscience*. https://doi.org/10.1046/j.1460-9568.2003.02928.x

Harauzov, A., Spolidoro, M., DiCristo, G., De Pasquale, R., Cancedda, L., Pizzorusso, T., … Maffei, L. (2010). Reducing intracortical inhibition in the adult visual cortex promotes ocular dominance plasticity. *Journal of Neuroscience*. https://doi.org/10.1523/JNEUROSCI.2233-09.2010

Hensch, T. K. (2005). Critical period plasticity in local cortical circuits. *Nature Reviews Neuroscience*. https://doi.org/10.1038/nrn1787

Hensch, T. K. (2005). Critical Period Mechanisms in Developing Visual Cortex. *Current Topics in Developmental Biology*. https://doi.org/10.1016/S0070-2153(05)69008-4

Hensch, T. K., Fagiolini, M., Mataga, N., Stryker, M. P., Baekkeskov, S., & Kash, S. F. (1998). Local GABA circuit control of experience-dependent plasticity in developing visual cortex. *Science*. https://doi.org/10.1126/science.282.5393.1504

Hiu, T., Farzampour, Z., Paz, J. T., Wang, E. H. J., Badgely, C., Olson, A., … Steinberg, G. K. (2016). Enhanced phasic GABA inhibition during the repair phase of stroke: A novel therapeutic target. *Brain*. https://doi.org/10.1093/brain/awv360

Huang, Z. J., Kirkwood, A., Pizzorusso, T., Porciatti, V., Morales, B., Bear, M. F., … Tonegawa, S. (1999). BDNF regulates the maturation of inhibition and the critical period of plasticity in mouse visual cortex. *Cell*. https://doi.org/10.1016/S0092-8674(00)81509-3

Hummel, F., Celnik, P., Giraux, P., Floel, A., Wu, W. H., Gerloff, C., & Cohen, L. G. (2005). Effects of non-invasive cortical stimulation on skilled motor function in chronic stroke. *Brain*. https://doi.org/10.1093/brain/awh369

Ito, U., Kuroiwa, T., Nagasao, J., Kawakami, E., & Oyanagi, K. (2006). Temporal profiles of axon terminals, synapses and spines in the ischemic penumbra of the cerebral cortex: Ultrastructure of neuronal remodeling. *Stroke*. https://doi.org/10.1161/01.STR.0000231875.96714.b1

Jablonka, J. A., Burnat, K., Witte, O. W., & Kossut, M. (2010). Remapping of the somatosensory cortex after a photothrombotic stroke: dynamics of the compensatory reorganization. *Neuroscience*. https://doi.org/10.1016/j.neuroscience.2009.09.074

Jackson, J., Ayzenshtat, I., Karnani, M. M., & Yuste, R. (2016). VIP+ interneurons control neocortical activity across brain states. *Journal of Neurophysiology*. https://doi.org/10.1152/jn.01124.2015

Kaneko, M., & Stryker, M. P. (2014). Sensory experience during locomotion promotes recovery of function in adult visual cortex. *ELife*. https://doi.org/10.7554/eLife.02798.001

Karagiannis, A., Gallopin, T., Dávid, C., Battaglia, D., Geoffroy, H., Rossier, J., … Cauli, B. (2009). Classification of NPY-expressing neocortical interneurons. *Journal of Neuroscience*. https://doi.org/10.1523/JNEUROSCI.0058-09.2009

Kato, N., Artola, A., & Singer, W. (1991). Developmental changes in the susceptibility to long-term potentiation of neurones in rat visual cortex slices. *Developmental Brain Research*. https://doi.org/10.1016/0165-3806(91)90153-A

Kerlin, A. M., Andermann, M. L., Berezovskii, V. K., & Reid, R. C. (2010). Broadly Tuned Response Properties of Diverse Inhibitory Neuron Subtypes in Mouse Visual Cortex. *Neuron*. https://doi.org/10.1016/j.neuron.2010.08.002

Kharlamov, E. A., Downey, K. L., Jukkola, P. I., Grayson, D. R., & Kelly, K. M. (2008). Expression of GABAA receptor α1 subunit mRNA and protein in rat neocortex following photothrombotic infarction. *Brain Research*. https://doi.org/10.1016/j.brainres.2008.02.070

Kim, S. Y., Hsu, J. E., Husbands, L. C., Kleim, J. A., & Jones, T. A. (2018). Coordinated plasticity of synapses and astrocytes underlies practice-driven functional vicariation in peri-infarct motor cortex. *Journal of Neuroscience*. https://doi.org/10.1523/JNEUROSCI.1295-17.2017

Kim, Y. H., You, S. H., Ko, M. H., Park, J. W., Lee, K. H., Jang, S. H., … Hallett, M. (2006). Repetitive transcranial magnetic stimulation-induced corticomotor excitability and associated motor skill acquisition in chronic stroke. *Stroke*. https://doi.org/10.1161/01.STR.0000221233.55497.51

Kirkwood, A., & Bear, M. F. (1994). Hebbian synapses in visual cortex. *Journal of Neuroscience*. https://doi.org/10.1523/jneurosci.14-03-01634.1994

Komatsu, Y. (1983). Development of cortical inhibition in kitten striate cortex investigated by a slice preparation. *Developmental Brain Research*. https://doi.org/10.1016/0165-3806(83)90165-7

Kuchibhotla, K. V., Gill, J. V., Lindsay, G. W., Papadoyannis, E. S., Field, R. E., Sten, T. A. H., … Froemke, R. C. (2017). Parallel processing by cortical inhibition enables context-dependent behavior. *Nature Neuroscience*. https://doi.org/10.1038/nn.4436

Lackland, D. T., Roccella, E. J., Deutsch, A. F., Fornage, M., George, M. G., Howard, G., … Towfighi, A. (2014). Factors influencing the decline in stroke mortality a statement from the american heart association/american stroke association. *Stroke*. https://doi.org/10.1161/01.str.0000437068.30550.cf

Lake, E. M. R., Chaudhuri, J., Thomason, L., Janik, R., Ganguly, M., Brown, M., … Stefanovic, B. (2015). The effects of delayed reduction of tonic inhibition on ischemic lesion and sensorimotor function. *Journal of Cerebral Blood Flow and Metabolism*. https://doi.org/10.1038/jcbfm.2015.86

Lee, S., Kruglikov, I., Huang, Z. J., Fishell, G., & Rudy, B. (2013). A disinhibitory circuit mediates motor integration in the somatosensory cortex. *Nature Neuroscience*. https://doi.org/10.1038/nn.3544

Luo, L., Callaway, E. M., & Svoboda, K. (2018). Genetic Dissection of Neural Circuits: A Decade of Progress. *Neuron*. https://doi.org/10.1016/j.neuron.2018.03.040

M. White, C., Ji, S., Cai, H., Maudsley, S., & Martin, B. (2012). Therapeutic Potential of Vasoactive Intestinal Peptide and its Receptors in Neurological Disorders. *CNS & Neurological Disorders - Drug Targets*. https://doi.org/10.2174/187152710793361595

Margolis, D. J., Lütcke, H., Schulz, K., Haiss, F., Weber, B., Kügler, S., … Helmchen, F. (2012). Reorganization of cortical population activity imaged throughout long-term sensory deprivation. *Nature Neuroscience*. https://doi.org/10.1038/nn.3240

Mostany, R., Chowdhury, T. G., Johnston, D. G., Portonovo, S. A., Carmichael, S. T., & Portera-Cailliau, C. (2010). Local hemodynamics dictate long-term dendritic plasticity in peri-infarct cortex. *Journal of Neuroscience*. https://doi.org/10.1523/JNEUROSCI.3908-10.2010

Nahirney, P. C., Reeson, P., & Brown, C. E. (2016). Ultrastructural analysis of blood-brain barrier breakdown in the peri-infarct zone in young adult and aged mice. *Journal of Cerebral Blood Flow and Metabolism*. https://doi.org/10.1177/0271678X15608396

Neumann-Haefelin, T., Hagemann, G., & Witte, O. W. (1995). Cellular correlates of neuronal hyperexcitability in the vicinity of photochemically induced cortical infarcts in rats in vitro. *Neuroscience Letters*. https://doi.org/10.1016/0304-3940(95)11677-O

Nitsche, M. A., Schauenburg, A., Lang, N., Liebetanz, D., Exner, C., Paulus, W., & Tergau, F. (2003). Facilitation of implicit motor learning by weak transcranial direct current stimulation of the primary motor cortex in the human. *Journal of Cognitive Neuroscience*. https://doi.org/10.1162/089892903321662994

Pfeffer, C. K., Xue, M., He, M., Huang, Z. J., & Scanziani, M. (2013). Inhibition of inhibition in visual cortex: The logic of connections between molecularly distinct interneurons. *Nature Neuroscience*. https://doi.org/10.1038/nn.3446

Pi, H. J., Hangya, B., Kvitsiani, D., Sanders, J. I., Huang, Z. J., & Kepecs, A. (2013). Cortical interneurons that specialize in disinhibitory control. *Nature*. https://doi.org/10.1038/nature12676

Porter, J. T., Cauli, B., Staiger, J. F., Lambolez, B., Rossier, J., & Audinat, E. (1998). Properties of bipolar VIPergic interneurons and their excitation by pyramidal

neurons in the rat neocortex. *European Journal of Neuroscience*. https://doi.org/10.1046/j.1460-9568.1998.00367.x

Prönneke, A., Scheuer, B., Wagener, R. J., Möck, M., Witte, M., & Staiger, J. F. (2015). Characterizing VIP neurons in the barrel cortex of VIPcre/tdTomato mice reveals layer-specific differences. *Cerebral Cortex*. https://doi.org/10.1093/cercor/bhv202

Que, M., Witte, O. W., Neumann-Haefelin, T., Schiene, K., Schroeter, M., & Zilles, K. (1999). Changes in GABA(A) and GABA(B) receptor binding following cortical photothrombosis: A quantitative receptor autoradiographic study. *Neuroscience*. https://doi.org/10.1016/S0306-4522(99)00197-9

Richards, C. D. (1983). Actions of general anaesthetics on synaptic transmission in the cns. *British Journal of Anaesthesia*. https://doi.org/10.1093/bja/55.3.201

Schiene, K., Bruehl, C., Zilles, K., Qü, M., Hagemann, G., Kraemer, M., & Witte, O. W. (1996). Neuronal hyperexcitability and reduction of GABA(A)-receptor expression in the surround of cerebral photothrombosis. *Journal of Cerebral Blood Flow and Metabolism*. https://doi.org/10.1097/00004647-199609000-00014

Seto, A., Taylor, S., Trudeau, D., Swan, I., Leung, J., Reeson, P., … Brown, C. E. (2014). Induction of ischemic stroke in awake freely moving mice reveals that isoflurane anesthesia can mask the benefits of a neuroprotection therapy. *Frontiers in Neuroenergetics*. https://doi.org/10.3389/fnene.2014.00001

Shoham, D., Glaser, D. E., Arieli, A., Kenet, T., Wijnbergen, C., Toledo, Y., … Grinvald, A. (1999). Imaging cortical dynamics at high spatial and temporal resolution with novel blue voltage-sensitive dyes. *Neuron*. https://doi.org/10.1016/S0896-6273(00)81027-2

Shoham, S., O'Connor, D. H., & Segev, R. (2006). How silent is the brain: Is there a "dark matter" problem in neuroscience? *Journal of Comparative Physiology A: Neuroethology, Sensory, Neural, and Behavioral Physiology*. https://doi.org/10.1007/s00359-006-0117-6

Spruston, N. (2008). Pyramidal neurons: Dendritic structure and synaptic integration. *Nature Reviews Neuroscience*. https://doi.org/10.1038/nrn2286

Staiger, J. F., Zilles, K., & Freund, T. F. (1996). Innervation of VIP-immunoreactive neurons by the ventroposteromedial thalamic nucleus in the barrel cortex of the rat. *Journal of Comparative Neurology*. https://doi.org/10.1002/(SICI)1096-9861(19960401)367:2<194::AID-CNE3>3.0.CO;2-0

Stroemer, R. P., Kent, T. A., & Hulsebosch, C. E. (1995). Neocortical neural sprouting, synaptogenesis, and behavioral recovery after neocortical infarction in rats. *Stroke*. https://doi.org/10.1161/01.STR.26.11.2135

Sugiyama, S., Di Nardo, A. A., Aizawa, S., Matsuo, I., Volovitch, M., Prochiantz, A., & Hensch, T. K. (2008). Experience-Dependent Transfer of Otx2 Homeoprotein into the Visual Cortex Activates Postnatal Plasticity. *Cell*. https://doi.org/10.1016/j.cell.2008.05.054

Takesian, A. E., Bogart, L. J., Lichtman, J. W., & Hensch, T. K. (2018). Inhibitory circuit gating of auditory critical-period plasticity. *Nature Neuroscience*. https://doi.org/10.1038/s41593-017-0064-2

Thévenaz, P., Ruttimann, U. E., & Unser, M. (1998). A pyramid approach to subpixel registration based on intensity. *IEEE Transactions on Image Processing*. https://doi.org/10.1109/83.650848

Thomas Carmichael, S., Wei, L., Rovainen, C. M., & Woolsey, T. A. (2001). New patterns of intracortical projections after focal cortical stroke. *Neurobiology of Disease*. https://doi.org/10.1006/nbdi.2001.0425

Tian, L., Hires, S. A., Mao, T., Huber, D., Chiappe, M. E., Chalasani, S. H., … Looger, L. L. (2009). Imaging neural activity in worms, flies and mice with improved GCaMP calcium indicators. *Nature Methods*. https://doi.org/10.1038/nmeth.1398

Uesugi, M., Kasuya, Y., Hama, H., Yamamoto, M., Hayashi, K., Masaki, T., & Goto, K. (1996). Endogenous endothelin-1 initiates astrocytic growth after spinal cord injury. *Brain Research*. https://doi.org/10.1016/0006-8993(96)00524-0

Uesugi, M., Kasuya, Y., Hayashi, K., & Goto, K. (1998). SB209670, a potent endothelin receptor antagonist, prevents or delays axonal degeneration after spinal cord injury. *Brain Research*. https://doi.org/10.1016/S0006-8993(97)01431-5

Veerbeek, J. M., Van Wegen, E., Van Peppen, R., Van Der Wees, P. J., Hendriks, E., Rietberg, M., & Kwakkel, G. (2014). What is the evidence for physical therapy poststroke? A systematic review and meta-analysis. *PLoS ONE*. https://doi.org/10.1371/journal.pone.0087987

Vetencourt, J. F. M., Sale, A., Viegi, A., Baroncelli, L., De Pasquale, R., O'Leary, O. F., … Maffei, L. (2008). The antidepressant fluoxetine restores plasticity in the adult visual cortex. *Science*. https://doi.org/10.1126/science.1150516

Wall, N. R., de la Parra, M., Sorokin, J. M., Taniguchi, H., Huang, Z. J., & Callaway, E. M. (2016). Brain-wide maps of synaptic input to cortical interneurons. *Journal of Neuroscience*. https://doi.org/10.1523/JNEUROSCI.3967-15.2016

Ward, N. S. (2017). Restoring brain function after stroke — bridging the gap between animals and humans. *Nature Reviews Neurology*. https://doi.org/10.1038/nrneurol.2017.34

Watson, B. D., Dietrich, W. D., Busto, R., Wachtel, M. S., & Ginsberg, M. D. (1985). Induction of reproducible brain infarction by photochemically initiated thrombosis. *Annals of Neurology*. https://doi.org/10.1002/ana.410170513

Winship, I. R. (2014). Laser speckle contrast imaging to measure changes in cerebral blood flow. *Methods in Molecular Biology*. https://doi.org/10.1007/978-1-4939-320-7_19

Winship, I. R., & Murphy, T. H. (2009). Remapping the somatosensory cortex after stroke: Insight from imaging the synapse to network. *Neuroscientist*. https://doi.org/10.1177/1073858409333076

Winship, I. R., & Murphy, T. H. (2008). In vivo calcium imaging reveals functional rewiring of single somatosensory neurons after stroke. *Journal of Neuroscience*. https://doi.org/10.1523/JNEUROSCI.0622-08.2008

Xerri, C., Merzenich, M. M., Peterson, B. E., & Jenkins, W. (1998). Plasticity of primary somatosensory cortex paralleling sensorimotor skill recovery from stroke in adult monkeys. *Journal of Neurophysiology*. https://doi.org/10.1152/jn.1998.79.4.2119

Xu, X., Roby, K. D., & Callaway, E. M. (2010). Immunochemical characterization of inhibitory mouse cortical neurons: Three chemically distinct classes of inhibitory cells. *Journal of Comparative Neurology*. https://doi.org/10.1002/cne.22229

Yazaki-Sugiyama, Y., Kang, S., Cteau, H., Fukai, T., & Hensch, T. K. (2009). Bidirectional plasticity in fast-spiking GABA circuits by visual experience. *Nature*. https://doi.org/10.1038/nature08485

Zepeda, A., Sengpiel, F., Guagnelli, M. A., Vaca, L., & Arias, C. (2004). Functional Reorganization of Visual Cortex Maps after Ischemic Lesions Is Accompanied by Changes in Expression of Cytoskeletal Proteins and NMDA and GABA A Receptor Subunits. *Journal of Neuroscience*. https://doi.org/10.1523/JNEUROSCI.3213-03.2004

Appendix

Table 1. Summary of statistical tests used in Figure 5 (repeated measures two-way ANOVA)

Low-intensity

Responsive cells %

Two-way repeated measures ANOVA		
Source of variation	F (DFn, DFd)	P-value
Time X Condition	F (3, 24) = 4.015	P=0.0190
Time	F (1.921, 15.37) = 3.590	P=0.0541
Condition	F (1, 8) = 5.964	P=0.0404
Multiple comparisons tests (Stroke-control)		
Stroke-Control	t values	P-value
Pre-stroke	0.4409	>0.9999
Week1	4.414	0.0205
week2	1.926	0.3665
week3	2.187	0.2425

Responsive trials %

Two-way repeated measures ANOVA		
Source of variation	F (DFn, DFd)	P-value
Time X Condition	F (3, 24) = 3.694	P=0.0257
Time	F (1.813, 14.50) = 3.992	P=0.0449
Condition	F (1, 8) = 4.605	P=0.0642
Multiple comparisons tests (Stroke-control)		
Stroke-Control	t values	P-value
Pre-stroke	0.1716	>0.9999
Week1	3.470	0.0675
week2	3.092	0.0619
week3	2.265	0.2255

Response amplitude dFo/Fo %

Two-way repeated measures ANOVA		
Source of variation	F (DFn, DFd)	P-value
Time X Condition	F (3, 24) = 2.876	P=0.0571
Time	F (1.687, 13.49) = 4.411	P=0.0387
Condition	F (1, 8) = 7.162	P=0.0281
Multiple comparisons tests (Stroke-control)		
Stroke-Control	t values	P-value
Pre-stroke	0.8258	>0.9999
Week1	2.841	0.1789
week2	2.447	0.1625
week3	2.821	0.1622

Low-intensity-normalized

Responsive cells %

Two-way repeated measures ANOVA		
Source of variation	F (DFn, DFd)	P-value
Time X Condition	F (3, 24) = 3.736	P=0.0247
Time	F (1.941, 15.53) = 3.333	P=0.0636
Condition	F (1, 8) = 12.28	P=0.0080
Multiple comparisons tests (Stroke-control)		
Stroke-Control	t values	P-value
Pre-stroke		
Week1	7.051	0.0006
week2	1.472	0.7588
week3	2.526	0.1935

Responsive trials %

Two-way repeated measures ANOVA		
Source of variation	F (DFn, DFd)	P-value
Time X Condition	F (3, 24) = 3.775	P=0.0238
Time	F (1.800, 14.40) = 3.523	P=0.0607
Condition	F (1, 8) = 13.13	P=0.0067
Multiple comparisons tests (Stroke-control)		
Stroke-Control	t values	P-value
Pre-stroke		
Week1	4.766	0.0061
week2	2.842	0.1321
week3	1.830	0.4975

Response amplitude dFo/Fo %

Two-way repeated measures ANOVA		
Source of variation	F (DFn, DFd)	P-value
Time X Condition	F (3, 24) = 3.381	P=0.0347
Time	F (1.667, 13.34) = 4.641	P=0.0346
Condition	F (1, 8) = 10.24	P=0.0126
Multiple comparisons tests (Stroke-control)		
Stroke-Control	t values	P-value
Pre-stroke		
Week1	6.328	0.0018
week2	0.7689	>0.9999
week3	2.735	0.1031

High-intensity

Responsive cells %

Two-way repeated measures ANOVA		
Source of variation	F (DFn, DFd)	P-value
Time X Condition	F (3, 24) = 1.447	P=0.2539
Time	F (1.765, 14.12) = 1.022	P=0.3759
Condition	F (1, 8) = 0.1860	P=0.6776
Multiple comparisons tests (Stroke-control)		
Stroke-Control	t values	P-value
Pre-stroke	0.8753	>0.9999
Week1	2.014	0.3574
week2	0.4624	>0.9999
week3	0.2245	>0.9999

Responsive trials %

Two-way repeated measures ANOVA		
Source of variation	F (DFn, DFd)	P-value
Time X Condition	F (3, 24) = 1.803	P=0.1736
Time	F (1.997, 15.98) = 1.348	P=0.2878
Condition	F (1, 8) = 2.049	P=0.1902
Multiple comparisons tests (Stroke-control)		
Stroke-Control	t values	P-value
Pre-stroke	0.4286	>0.9999
Week1	3.878	0.0695
week2	1.286	0.9422
week3	0.6508	>0.9999

Response amplitude dFo/Fo %

Two-way repeated measures ANOVA		
Source of variation	F (DFn, DFd)	P-value
Time X Condition	F (3, 24) = 0.9220	P=0.4452
Time	F (1.503, 12.03) = 1.147	P=0.3332
Condition	F (1, 8) = 0.04691	P=0.8340
Multiple comparisons tests (Stroke-control)		
Stroke-Control	t values	P-value
Pre-stroke	0.2611	>0.9999
Week1	3.621	0.0941
week2	0.3178	>0.9999
week3	0.03443	>0.9999

High-intensity-normalized

Responsive cells %

Two-way repeated measures ANOVA		
Source of variation	F (DFn, DFd)	P-value
Time X Condition	F (3, 24) = 1.248	P=0.3142
Time	F (1.918, 15.34) = 0.873	P=0.4333
Condition	F (1, 8) = 3.324	P=0.1057
Multiple comparisons tests (Stroke-control)		
Stroke-Control	t values	P-value
Pre-stroke		
Week1	2.935	0.0903
week2	0.9635	>0.9999
week3	1.275	0.9544

Responsive trials %

Two-way repeated measures ANOVA		
Source of variation	F (DFn, DFd)	P-value
Time X Condition	F (3, 24) = 1.741	P=0.1853
Time	F (2.322, 18.57) = 1.377	P=0.2790
Condition	F (1, 8) = 1.825	P=0.2137
Multiple comparisons tests (Stroke-control)		
Stroke-Control	t values	P-value
Pre-stroke		
Week1	2.751	0.1001
week2	0.5995	>0.9999
week3	0.7628	>0.9999

Response amplitude dFo/Fo %

Two-way repeated measures ANOVA		
Source of variation	F (DFn, DFd)	P-value
Time X Condition	F (3, 24) = 1.560	P=0.2249
Time	F (2.216, 17.73) = 0.887	P=0.4391
Condition	F (1, 8) = 1.103	P=0.3244
Multiple comparisons tests (Stroke-control)		
Stroke-Control	t values	P-value
Pre-stroke		
Week1	2.094	0.2961
week2	0.04146	>0.9999
week3	1.175	>0.9999

Table 2. Summary of statistical tests used in Figure 5 (repeated measures one-way ANOVA)

Low-intensity

Responsive cells %			
One-way repeated measures ANOVA			
Source of variation	F (DFn, DFd)	P-value	
Time	F (2.520, 12.10) = 4.505	0.0284	
Multiple comparisons tests			
Stroke-Control	t values	P-value	
Pre-stroke Vs. PS1	9.548	0.0007	
Pre-stroke Vs. PS2	1.615	0.4453	
Pre-stroke Vs. PS3	2.449	0.1766	
Pre-stroke Vs. PS4	3.968	0.0355	
Pre-stroke Vs. PS5	4.153	0.0444	

Responsive trials %			
One-way repeated measures ANOVA			
Source of variation	F (DFn, DFd)	P-value	
Time	F (2.456, 11.79) = 4.226	0.0354	
Multiple comparisons tests			
Stroke-Control	t values	P-value	
Pre-stroke Vs. PS1	6.144	0.0058	
Pre-stroke Vs. PS2	2.850	0.1130	
Pre-stroke Vs. PS3	2.461	0.1743	
Pre-stroke Vs. PS4	3.358	0.0655	
Pre-stroke Vs. PS5	3.062	0.1126	

Response amplitude (dF/Fo) %			
One-way repeated measures ANOVA			
Source of variation	F (DFn, DFd)	P-value	
Time	F (2.393, 11.49) = 4.950	0.0240	
Multiple comparisons tests			
Stroke-Control	t values	P-value	
Pre-stroke Vs. PS1	5.498	0.0094	
Pre-stroke Vs. PS2	1.584	0.4601	
Pre-stroke Vs. PS3	3.382	0.0639	
Pre-stroke Vs. PS4	2.555	0.1567	
Pre-stroke Vs. PS5	3.229	0.0967	

Low-intensity-normalized

Responsive cells %			
One-way repeated measures ANOVA			
Source of variation	F (DFn, DFd)	P-value	
Time	F (2.390, 11.47) = 4.221	0.0371	
Multiple comparisons tests			
Stroke-Control	t values	P-value	
Pre-stroke Vs. PS1	7.777	0.0020	
Pre-stroke Vs. PS2	1.272	0.6242	
Pre-stroke Vs. PS3	2.423	0.1818	
Pre-stroke Vs. PS4	3.975	0.0353	
Pre-stroke Vs. PS5	4.704	0.0293	

Responsive trials %			
One-way repeated measures ANOVA			
Source of variation	F (DFn, DFd)	P-value	
Time	F (2.413, 11.58) = 4.040	0.0410	
Multiple comparisons tests			
Stroke-Control	t values	P-value	
Pre-stroke Vs. PS1	5.349	0.0105	
Pre-stroke Vs. PS2	3.252	0.0732	
Pre-stroke Vs. PS3	2.415	0.1835	
Pre-stroke Vs. PS4	3.623	0.0499	
Pre-stroke Vs. PS5	2.298	0.2349	

Response amplitude (dF/Fo) %			
One-way repeated measures ANOVA			
Source of variation	F (DFn, DFd)	P-value	
Time	F (2.501, 12.01) = 4.750	0.0247	
Multiple comparisons tests			
Stroke-Control	t values	P-value	
Pre-stroke Vs. PS1	7.610	0.0022	
Pre-stroke Vs. PS2	1.560	0.4713	
Pre-stroke Vs. PS3	4.001	0.0344	
Pre-stroke Vs. PS4	2.867	0.1109	
Pre-stroke Vs. PS5	3.185	0.1005	

High-intensity

Responsive cells %			
One-way repeated measures ANOVA			
Source of variation	F (DFn, DFd)	P-value	
Time	F (2.768, 13.29) = 1.506	0.2587	
Multiple comparisons tests			
Stroke-Control	t values	P-value	
Pre-stroke Vs. PS1	2.616	0.1464	
Pre-stroke Vs. PS2	1.068	0.7404	
Pre-stroke Vs. PS3	1.019	0.7679	
Pre-stroke Vs. PS4	1.346	0.5830	
Pre-stroke Vs. PS5	0.8019	0.8777	

Responsive trials %			
One-way repeated measures ANOVA			
Source of variation	F (DFn, DFd)	P-value	
Time	F (2.377, 11.41) = 1.872	0.1955	
Multiple comparisons tests			
Stroke-Control	t values	P-value	
Pre-stroke Vs. PS1	2.800	0.1194	
Pre-stroke Vs. PS2	1.028	0.7629	
Pre-stroke Vs. PS3	1.105	0.7196	
Pre-stroke Vs. PS4	0.7709	0.8934	
Pre-stroke Vs. PS5	0.8484	0.8563	

Response amplitude (dF/Fo) %		
One-way repeated measures ANOVA		
Source of variation	F (DFn, DFd)	P-value
Time	F (1.408, 6.759) = 1.174	0.3417
Multiple comparisons tests		
Stroke-Control	t values	P-value
Pre-stroke Vs. PS1	1.649	0.4297
Pre-stroke Vs. PS2	0.8533	0.8555
Pre-stroke Vs. PS3	2.397	0.1873
Pre-stroke Vs. PS4	1.021	0.7672
Pre-stroke Vs. PS5	0.8135	0.8725

High-intensity-normalized

Responsive cells %			
One-way repeated measures ANOVA			
Source of variation	F (DFn, DFd)	P-value	
Time	F (2.803, 13.45) = 1.234	0.3339	
Multiple comparisons tests			
Stroke-Control	t values	P-value	
Pre-stroke Vs. PS1	2.868	0.1107	
Pre-stroke Vs. PS2	0.7010	0.9214	
Pre-stroke Vs. PS3	0.9602	0.8004	
Pre-stroke Vs. PS4	1.227	0.6494	
Pre-stroke Vs. PS5	0.7951	0.8808	

Responsive trials %			
One-way repeated measures ANOVA			
Source of variation	F (DFn, DFd)	P-value	
Time	F (2.682, 12.87) = 1.896	0.1835	
Multiple comparisons tests			
Stroke-Control	t values	P-value	
Pre-stroke Vs. PS1	3.329	0.0676	
Pre-stroke Vs. PS2	0.7627	0.8970	
Pre-stroke Vs. PS3	1.204	0.6628	
Pre-stroke Vs. PS4	0.5458	0.9679	
Pre-stroke Vs. PS5	0.6250	0.9450	

Response amplitude (dF/Fo) %			
One-way repeated measures ANOVA			
Source of variation	F (DFn, DFd)	P-value	
Time	F (2.720, 13.06) = 1.416	0.2820	
Multiple comparisons tests			
Stroke-Control	t values	P-value	
Pre-stroke Vs. PS1	2.912	0.1056	
Pre-stroke Vs. PS2	0.5957	0.9555	
Pre-stroke Vs. PS3	1.845	0.3478	
Pre-stroke Vs. PS4	0.7348	0.9084	
Pre-stroke Vs. PS5	1.193	0.6745	